electronics

MDPI

Article

Modified SVPWM-Based Fault-Tolerant Operation of a Seven-Phase PMSM Drive After Two-Phase Open-Circuit Fault

Kamel Saleh

Electrical Engineering Department, Faculty of Engineering, New Campus, An-Najah National University, Nablus P.O. Box 7, Palestine; kamel.saleh@najah.edu

Abstract

This article presents a novel fault-tolerant control (FTC) scheme for a seven-phase PMSM drive to enhance its performance when two phases experience an open-circuit failure at the same time. For example, phases "a" and "b" are considered first-neighbor phases, "a" and "c" are second-neighbor phases, and "a" and "d" are third-neighbor phases. This approach makes the drive system more reliable and helps to reduce torque and speed fluctuations. To maintain the Magnetomotive Force (MMF) and improve overall performance, the FTC method focuses on controlling the current's magnitude and angle after the faults. The process starts by calculating the angles and magnitudes after the fault occurs in each scenario. Based on this new current distribution, a specific multidimensional SVPWM technique is designed for each fault case. When simulating the fault in phases "a" and "b", the torque ripple decreased from 0.4 N·m to 0.1 N·m, and the speed ripple dropped from 10 rpm to 4 rpm after applying the new FTC. For the fault in phases "a" and "c", the torque ripple went down from 0.25 N·m to 0.1 N·m, and the speed ripple reduced from 2 rpm to 0.3 rpm with the new FTC. In the case of a fault in phases "a" and "d", the torque ripple was cut from 0.6 N·m to 0.2 N·m, and the speed ripple dropped from 5 rpm to 0.5 rpm after implementing the new FTC. Furthermore, the dynamic performance of the motor during faults and during changes in speed and load was just as good as when the motor was operating normally.

Keywords: multi-phase motor; open-circuit faults; SVPWM

1. Introduction

Multi-phase machines offer significant advantages in various commercial uses. They are used in situations where a consistent high power output is needed, allowing for high torque and power even with large currents, without increasing voltage or current, as seen in electric marine systems. They are also used in applications that require low torque and minimal speed fluctuations, such as electric vehicles. Additionally, these machines are utilized in systems that need a high level of reliability with built-in fault tolerance, including electric aircraft [1–3]. Phase redundancy (open-circuit and short-circuit faults) gives an inherent fault-tolerant capability for multi-phase motor drives, enabling autonomous work without additional hardware [4–7]. The ability to operate normally on two of the three phases is a distinct advantage over conventional three-phase machines. This capability is particularly interesting for EV and aerospace fault-tolerant propulsion research.

Although open-phase faults are the most commonly studied type in multi-phase drives, other fault types, such as short-circuit faults, inverter switch failures, and sensor faults, are also being researched [4,5,8,9].

Check for updates

Academic Editors: Fabio Corti and Dorin Petreus

Received: 8 September 2026
Revised: 24 October 2026
Accepted: 2 November 2026
Published: 6 November 2026

Copyright: © 2026 by the author. Licensee MDPI, Basel, Switzerland. This article is an open access article distributed under the terms and conditions of the Creative Commons Attribution (CC BY) license.

Multi-phase motor drives find use in automotive, marine, wind energy, and industrial sectors. However, aerospace and electric vehicles are the main areas of research for fault-tolerant multi-phase drives [4,10]. These studies primarily focus on the stability of the motor drive after open-circuit or short-circuit faults, which is crucial for passenger safety. Most of the research is centered around nine-phase configurations and control strategies for post-fault operation. Fault-tolerant control strategies involve several steps, including detecting and locating faults, followed by reconfiguring transformation matrices and current references [5,11]. After the fault, the healthy currents are typically controlled to achieve maximum torque, minimum losses, and balanced current flow [7,12]. It is important to note that the distribution of stator currents after a fault can be calculated offline using the mathematical model of the multi-phase machine. However, to adjust the current distribution based on FTC techniques, various controllers have been used in the literature. Some studies used hysteresis current controllers for FTC [13–15], but they have limited application due to their variable switching frequency. Another technique used is vector control, alongside modified space vector pulse width modulation (SVPWM) [16,17]. Other approaches include using a new transformation matrix that takes into account the new current distribution after a fault [18–22]. Additionally, other control methods such as model predictive control [23], direct torque control [24], and sliding mode control have also been applied post-fault [25].

Adaptive fault-tolerant control (AFTC) serves as a tool for restoring normal and optimal operation. AFTC can enhance diagnosis accuracy and prevent misdiagnosis by matching actual operational data with theoretical models [26]. Recent work also explores online fault detection using artificial intelligence and machine learning methods, allowing for corrective actions before system failure [10]. Emerging trends include passive fault tolerance to reduce detection delays, adaptive control to avoid fault localization, and integrated hardware–software fault-tolerant systems that combine real-time diagnostics with corrective actions [5,10].

Healthy Operation of a Seven-Phase Drive

For a seven-phase motor operating under healthy conditions, the distribution of the stator currents is described by Equation (1), Figure 1a,b [27–30], where $\bar{I}m$ represents the peak value of the current in any phase, $\psi = 2\pi/7$, and Ω represents the angular frequency.

$$\begin{bmatrix} i a_h \\ i b_h \\ i c_h \\ i d_h \\ i e_h \\ i f_h \\ i g_h \end{bmatrix} = \begin{bmatrix} \bar{I}_m * \cos(\Omega t) \\ \bar{I}_m * \cos(\Omega t - \psi) \\ \bar{I}_m * \cos(\Omega t - 2\psi) \\ \bar{I}_m * \cos(\Omega t - 3\psi) \\ \bar{I}_m * \cos(\Omega t - 4\psi) \\ \bar{I}_m * \cos(\Omega t - 5\psi) \\ \bar{I}_m * \cos(\Omega t - 6\psi) \end{bmatrix} \quad (1)$$

The current in each phase creates a Magnetomotive Force (MMF), and the total MMF in the stator is shown in Equation (2). This total depends on the peak of the stator currents ($\bar{I}m$), the spatial angle (φ), and the total number of turns for each phase (N).

$$MMF_{total}(\varphi, t) = \frac{7}{8} * N * \bar{I}m * \left(e^{i\Omega t} * e^{-i\varphi} + e^{-i\Omega t} * e^{i\varphi}\right) \quad (2)$$

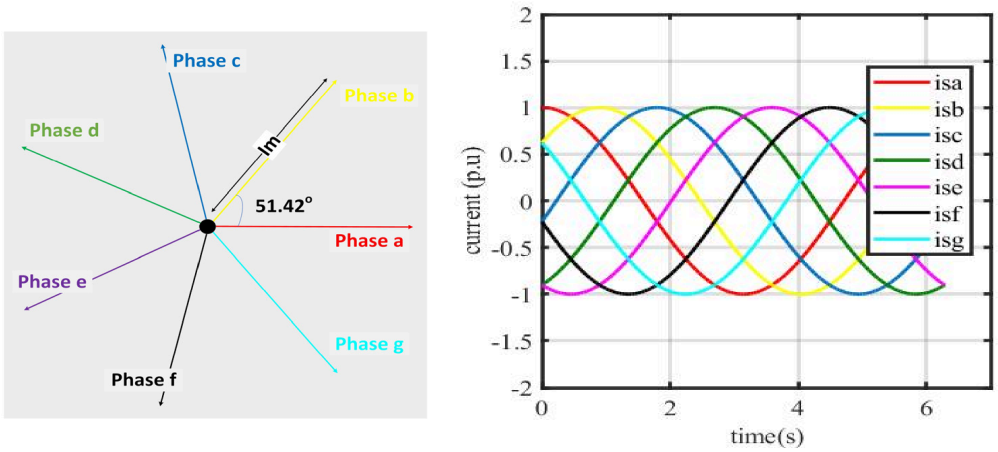

(**a**) (**b**)

Figure 1. Distribution of the currents in the seven-phase motor running normally. (**a**) Phasor; (**b**) sinusoidal.

The total of all the MMFs in the stator can also be calculated using the stator currents, as shown in Equation (3).

$$MMF_{total}(\varphi,\Omega t) = \frac{N}{4} * \left(e^{i\varphi}\left(\imath a_h + \imath b_h * e^{i\psi} + \imath c_h * e^{2i\psi} + \imath d_h * e^{3i\psi} + \imath e_h * e^{4i\psi} + \imath f_h * e^{5i\psi} + \imath g_h * e^{6i\psi}\right) + e^{-i\varphi}\left(\imath a_h + \imath b_h * e^{i\psi} + \imath c_h * e^{2i\psi} + \imath d_h * e^{3i\psi} + \imath e_h * e^{4i\psi} + \imath f_h * e^{5i\psi} + \imath g_h * e^{6i\psi}\right)\right) \quad (3)$$

By equating Equations (2) and (3), the following equation can be expressed:

$$\frac{7}{2} * \bar{I}m * e^{i\Omega t} = \imath a_h + \imath b_h * e^{i\psi} + \imath c_h * e^{2i\psi} + \imath d_h * e^{3i\psi} + \imath e_h * e^{4i\psi} + \imath f_h * e^{5i\psi} + \imath g_h * e^{6i\psi} \quad (4)$$

If an open-circuit fault occurs during the operation of a seven-phase motor drive, it is important to use a good fault-tolerant control method to keep the system working well after the fault. This is done by keeping the total torque-producing magnetic field (MMF) the same after the fault, without needing a neutral line to ensure the system runs safely. Therefore, Equation (4) is used to calculate the new distribution of the remaining healthy stator currents after the open-circuit fault, regardless of how many phases are affected. In this paper, the cases where two phases are experiencing an open-circuit fault at the same time are researched. If the fault happens in first-neighboring phases, like phases 'a' and 'b', it is called a 'type-I two-phase failure'. If the fault occurs in second-neighbor phases, like phases 'a' and 'c', it is referred to as a 'type-II two-phase failure'. Finally, if the fault happens in third-neighbor phases, like phases 'a' and 'd', it is known as a 'type-III two-phase failure'.

2. Operation of Seven-Phase Drive Under Two-Phase Open-Circuit Fault

2.1. Type-I Two-Phase Failure

If a seven-phase drive experiences a type-I two-phase failure, like when phases 'a' and 'b' become open-circuit, the way the remaining healthy currents are distributed after the fault is shown in Equation (5):

$$\begin{bmatrix} \imath a_{_fault-ab} \\ \imath b_{_fault-ab} \\ \imath c_{_fault-ab} \\ \imath d_{_fault-ab} \\ \imath e_{_fault-ab} \\ \imath f_{_fault-ab} \\ \imath g_{_fault-ab} \end{bmatrix} = I_{fault-ab} * \begin{bmatrix} 0 \\ 0 \\ \cos\left(\Omega t - \phi_{c-fault-ab}\right) \\ \cos\left(\Omega t - \phi_{d-fault-ab}\right) \\ \cos\left(\Omega t - \phi_{e-fault-ab}\right) \\ \cos\left(\Omega t - \phi_{f-fault-ab}\right) \\ \cos\left(\Omega t - \phi_{g-fault-ab}\right) \end{bmatrix} \quad (5)$$

where $I_{fault-ab}$ represents the amplitude of the remaining healthy currents, and $\phi_{c-fault-ab}$, $\phi_{d-fault-ab}$, $\phi_{e-fault-ab}$, $\phi_{f-fault-ab}$, and $\phi_{g-faul-ab}$ are the new angles of the remaining healthy currents $ic_{-fault-ab}$, $id_{-fault-ab}$, $ie_{-fault-ab}$, $if_{-fault-ab}$, and $ig_{-fault-ab}$ respectively. To find out the above variables, i.e., ($I_{fault-ab}$, $\phi_{c-fault-ab}$, $\phi_{d-fault-ab}$, $\phi_{e-fault-ab}$, $\phi_{f-fault-ab}$, and $\phi_{g-fault-ab}$), and thus find out the new distribution of the stator current in the case of a type-I two-phase fault, the following steps are carried out.

Firstly, Equation (5) is substituted into Equation (4), yielding:

$$\frac{7}{2} * \bar{I}m * e^{i\Omega t} = e^{2i\psi} * (ic_{-fault-ab} + id_{-fault-ab} * e^{i\psi} + ie_{-fault-ab} * e^{2i\psi} + if_{-fault-ab} * e^{3i\psi} + ig_{-fault-ab} * e^{4i\psi} \quad (6)$$

Then, Equation (6) can be expressed using trigonometric formulas as follows:

$$\frac{7}{2} * \bar{I}m = I_{fault-ab} * \left((\cos 2\psi) * \cos\left(\phi_{c-fault-ab}\right) + (\cos 3\psi) * \cos\left(\phi_{d-fault-ab}\right) + (\cos 4\psi) * \cos\left(\phi_{e-fault-ab}\right) + (\cos 5\psi) * \cos\left(\phi_{f-fault-ab}\right) + (\cos 6\psi) * \cos\left(\phi_{g-fault-ab}\right)\right) \quad (7)$$

$$0 = I_{fault-ab} * ((\cos 2\psi) * \sin(\phi_{c-fault-ab}) + (\cos 3\psi) * \sin(\phi_{d-fault-ab}) + (\cos 4\psi) * \sin(\phi_{e-fault-ab}) + (\cos 5\psi) * \sin(\phi_{f-fault-ab}) + (\cos 6\psi) * \sin(\phi_{g-fault-ab})) \quad (8)$$

$$\frac{7}{2} * \bar{I}m = I_{fault-ab} * \left((\sin 2\psi) * \sin\left(\phi_{c-fault-ab}\right) + (\sin 3\psi) * \sin\left(\phi_{d-fault-ab}\right) + (\sin 4\psi) * \sin\left(\phi_{e-fault-ab}\right) + (\sin 5\psi) * \sin\left(\phi_{f-fault-ab}\right) + (\sin 6\psi) * \sin\left(\phi_{g-fault-ab}\right)\right) \quad (9)$$

$$0 = I_{fault-ab} * ((\sin 2\psi) * \cos(\phi_{c-fault-ab}) + (\sin 3\psi) * \cos(\phi_{d-fault-ab}) + (\sin 4\psi) * \cos(\phi_{e-fault-ab}) + (\sin 5\psi) * \cos(\phi_{f-fault-ab}) + (\sin 6\psi) * \cos(\phi_{g-fault-ab})) \quad (10)$$

Also, to keep the neutral current equal to zero after the fault, the following two equations can be deduced:

$$0 = \cos(\phi_{c-fault-ab}) + \cos(\phi_{d-fault-ab}) + \cos(\phi_{e-fault-ab}) + \cos(\phi_{f-fault-ab}) + \cos(\phi_{g-fault-ab}) \quad (11)$$

$$0 = \sin(\phi_{c-fault-ab}) + \sin(\phi_{d-fault-ab}) + \sin(\phi_{e-fault-ab}) + \sin(\phi_{f-fault-ab}) + \sin(\phi_{g-fault-ab}) \quad (12)$$

Finally, solving Equations (7)–(12) using the 'vpasolve ()' function in Matlab yields the new distribution of the remaining stator currents in the case of the failure in phases 'a' and 'b' as shown in Equation (13) and Figure 2a,b.

$$\begin{bmatrix} ia_{-fault-ab} \\ ib_{-fault-ab} \\ ic_{-fault-ab} \\ id_{-fault-ab} \\ ie_{-fault-ab} \\ if_{-fault-ab} \\ ig_{-fault-ab} \end{bmatrix} = \begin{bmatrix} 0 \\ 0 \\ 1.761 * \bar{I}m * \cos(\Omega t - 43.5°) \\ 1.761 * \bar{I}m * \cos(\Omega t - 142.6°) \\ 1.761 * \bar{I}m * \cos(\Omega t - 205.7°) \\ 1.761 * \bar{I}m * \cos(\Omega t - 268.8°) \\ 1.761 * \bar{I}m * \cos(\Omega t - 368.0°) \end{bmatrix} \quad (13)$$

In general, the fault-tolerant procedures that should be done to the stator currents under a type-I two-phase failure like phase 'a' and 'b' in order to maintain the performance are illustrated in Figure 3. First, the current in the remaining stator phase should be increased by 76%. Then, the two healthy neighbor phases, which are 'c' and 'g', should be shifted towards the faulty phases by 60°. Next, the following two healthy phases, 'd' and 'f', should also be shifted towards the faulty phases by 11.7°. Finally, the healthy phase 'e', which is opposite to the faulty phases, should remain unchanged. This approach can be applied to all similar type-I two-phase faults, such as those between 'a' and 'g', 'b' and 'c', and so on.

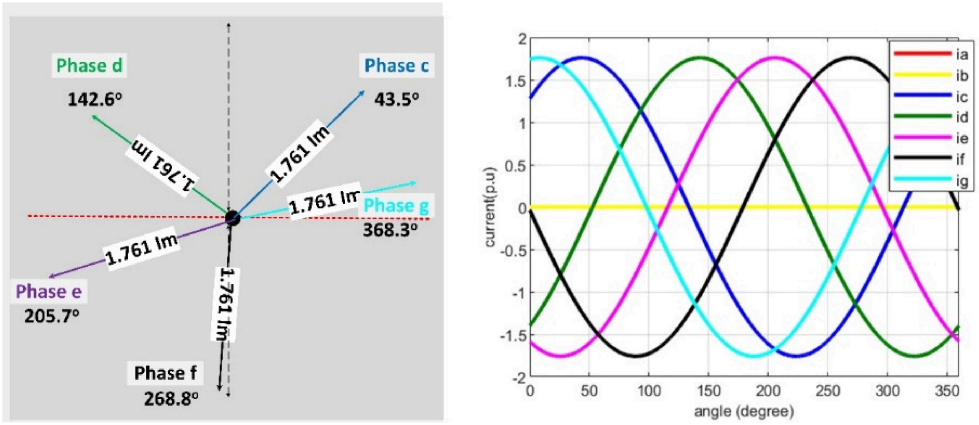

Figure 2. Distribution of the currents in the seven-phase motor running under type-I two-phase failure. (**a**) Phasor; (**b**) sinusoidal.

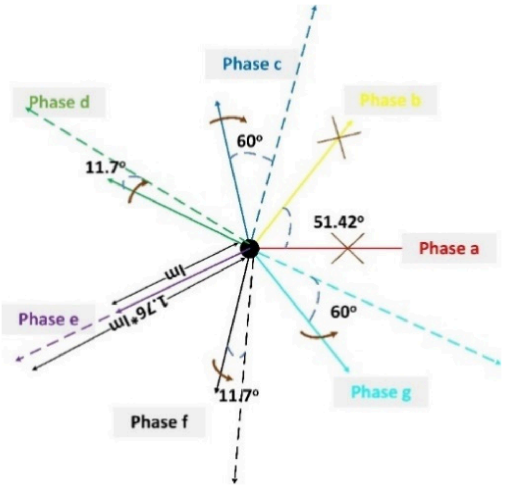

Figure 3. Phasor diagram illustrating the phase shift introduced to remaining healthy phase under type-I two-phase failure.

2.2. Type-II Two-Phase Failure

If a seven-phase drive is exposed to a type-II two-phase failure (i.e., phases 'a' and 'c' become open-circuit as an example), the distribution of the remaining healthy currents after the fault is given in Equation (14).

$$\begin{bmatrix} i a_{-fault-ac} \\ i b_{-fault-ac} \\ i c_{-fault-ac} \\ i d_{-fault-ac} \\ i e_{-fault-ac} \\ i f_{-fault-ac} \\ i g_{-fault-ac} \end{bmatrix} = I_{fault-ac} * \begin{bmatrix} 0 \\ \cos\left(\Omega t - \phi_{b-fault-ac}\right) \\ 0 \\ \cos\left(\Omega t - \phi_{d-fault-ac}\right) \\ \cos\left(\Omega t - \phi_{e-fault-ac}\right) \\ \cos\left(\Omega t - \phi_{f-fault-ac}\right) \\ \cos\left(\Omega t - \phi_{g-fault-ac}\right) \end{bmatrix} \quad (14)$$

where $I_{fault-ac}$ represents the amplitude of the remaining healthy currents, and $\phi_{b-fault-ac}$, $\phi_{d-fault-ac}$, $\phi_{e-fault-ac}$, $\phi_{f-fault-ac}$, and $\phi_{g-fault-ac}$ are the new angles of the remaining healthy currents $ib_{-fault-ac}$, $id_{-fault-ac}$, $ie_{-fault-ac}$, $if_{-fault-ac}$, and $ig_{-fault-ac}$ respectively. To find out the above variables, i.e., ($I_{fault-ac}$, $\phi_{b-fault-ac}$, $\phi_{d-fault-ac}$, $\phi_{e-fault-ac}$, $\phi_{f-fault-ac}$, and $\phi_{g-fault-ac}$), and thus find out the new distribution of the stator current in the case of a type-II two-phase fault, the following steps are carried out.

Firstly, Equation (4) is substituted into Equation (14), yielding:

$$\frac{7}{2} * \bar{I}m * e^{i\Omega t} = e^{i\psi} * (ib_{-fault-ac} + id_{-fault-ac} * e^{2i\psi} + ie_{-fault-ac} * e^{3i\psi} + if_{-fault-ac} * e^{4i\psi} + ig_{-fault-ac} * e^{5i\psi} \quad (15)$$

Then, Equation (15) can be expressed using trigonometric formulas as follows:

$$\frac{7}{2} * \bar{I}m = I_{fault_ac} * \left((\cos\psi) * \cos\left(\phi_{b-fault-ac}\right) + (\cos 3\psi) * \cos\left(\phi_{d-fault-ac}\right) + (\cos 4\psi) * \cos\left(\phi_{e-fault-ac}\right) + (\cos 5\psi) * \cos\left(\phi_{f-fault-ac}\right) + (\cos 6\psi) * \cos\left(\phi_{g-fault-ac}\right)\right) \quad (16)$$

$$0 = I_{fault-ac} * ((\cos\psi) * \sin(\phi_{b-fault-ac}) + (\cos 3\psi) * \sin(\phi_{d-fault-ac}) + (\cos 4\psi) * \sin(\phi_{e-fault-ac}) + (\cos 5\psi) * \sin(\phi_{f-fault-ac}) + (\cos 6\psi) * \sin(\phi_{g-fault-ac})) \quad (17)$$

$$\frac{7}{2} * \bar{I}m = I_{fault-ac} * \left((\sin\psi) * \sin\left(\phi_{b-fault-ac}\right) + (\sin 3\psi) * \sin\left(\phi_{d-fault-ac}\right) + (\sin 4\psi) * \sin\left(\phi_{e-fault-ac}\right) + (\sin 5\psi) * \sin\left(\phi_{f-fault-ac}\right) + (\sin 6\psi) * \sin\left(\phi_{g-fault-ac}\right)\right) \quad (18)$$

$$0 = I_{fault-ac} * ((\sin\psi) * \cos(\phi_{b-fault-ac}) + (\sin 3\psi) * \cos(\phi_{d-fault-ac}) + (\sin 4\psi) * \cos(\phi_{e-fault-ac}) + (\sin 5\psi) * \cos(\phi_{f-fault-ac}) + (\sin 6\psi) * \cos(\phi_{g-fault-ac})) \quad (19)$$

Also, to keep the neutral current equal to zero after the faults, the following two equations can be deduced:

$$0 = \cos(\phi_{b-fault-ac}) + \cos(\phi_{d-fault-ac}) + \cos(\phi_{e-fault-ac}) + \cos(\phi_{f-fault-ac}) + \cos(\phi_{g-fault-ac}) \quad (20)$$

$$0 = \sin(\phi_{b-fault-ac}) + \sin(\phi_{d-fault-ac}) + \sin(\phi_{e-fault-ac}) + \sin(\phi_{f-fault-ac}) + \sin(\phi_{g-fault-ac}) \quad (21)$$

Finally, solving equations (16)–(21) using 'vpasolve ()' function in MATLAB yields the new distribution of the remaining stator currents in the case of the failure in phases 'a' and 'c' as shown in Equation (22) and Figure 4a,b:

$$\begin{bmatrix} ia_{-fault\ ac} \\ ib_{-fault\ ac} \\ ic_{-fault\ ac} \\ id_{-fault\ ac} \\ ie_{-fault\ ac} \\ if_{-fault\ ac} \\ ig_{-fault\ ac} \end{bmatrix} = \begin{bmatrix} 0 \\ 1.497 * \bar{I}m * \cos(\omega t - 51.4°) \\ 0 \\ 1.497 * \bar{I}m * \cos(\omega t - 122.6°) \\ 1.497 * \bar{I}m * \cos(\omega t - 196.8°) \\ 1.497 * \bar{I}m * \cos(\omega t - 266.1°) \\ 1.497 * \bar{I}m * \cos(\omega t - 340.3°) \end{bmatrix} \quad (22)$$

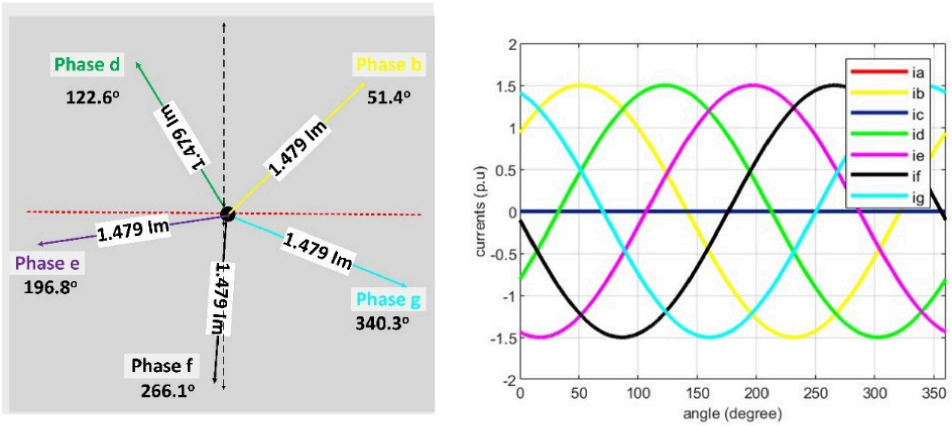

(**a**) (**b**)

Figure 4. Distribution of the currents in the seven-phase motor running under a type-II two-phase failure. (**a**) Phasor; (**b**) sinusoidal.

In conclusion, Figure 5 shows the fault-tolerant procedures that should be done to the stator currents under a type-II two-phase failure, i.e., ('a' and 'c'), in order to maintain the performance. First, the current in the remaining stator phase should be increased by 49.7%. Phase 'b' that is between the faulty phases should be shifted. Additionally, the two adjacent phases, 'd' and 'g', should be shifted closer to the faulty phases by 31.7°. Finally, the next two phases, 'e' and 'f', should be shifted toward the faulty phases by 8.9°. This approach can be applied to all similar cases where faults occur in second-adjacent phases, such as phases 'a' and 'f', 'b' and 'd', and so on.

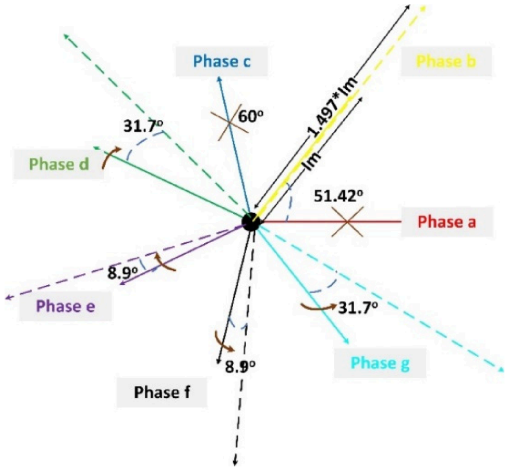

Figure 5. Phasor diagram illustrating the phase shift introduced to remaining healthy phase under a type-II two-phase failure.

2.3. Type-III Two-Phase Failure

If a seven-phase drive is exposed to a type-III two-phase failure (i.e., phases 'a' and 'd' become open-circuit as an example), the distribution of the remaining healthy currents after the fault is given in Equation (23):

$$\begin{bmatrix} i a_{-fault-ad} \\ i b_{-fault-ad} \\ i c_{-fault-ad} \\ i d_{-fault-ad} \\ i e_{-fault-ad} \\ i f_{-fault-ad} \\ i g_{-fault-ad} \end{bmatrix} = I_{fault-ad} * \begin{bmatrix} 0 \\ \cos\left(\Omega t - \phi_{b-fault-ad}\right) \\ \cos\left(\Omega t - \phi_{c-fault-ad}\right) \\ 0 \\ \cos\left(\Omega t - \phi_{e-fault-ad}\right) \\ \cos\left(\Omega t - \phi_{f-fault-ad}\right) \\ \cos\left(\Omega t - \phi_{g-fault-ad}\right) \end{bmatrix} \quad (23)$$

where $I_{fault-ad}$ represents the amplitude of the remaining healthy currents, and $\phi_{b-fault-ad}$, $\phi_{c-fault-ad}$, $\phi_{e-fault-ad}$, $\phi_{f-fault-ad}$, and $\phi_{g-fault-ad}$ are the new angles of the remaining healthy currents $ib_{-fault-ad}$, $ic_{-fault-ad}$, $ie_{-fault-ad}$, $if_{-fault-ad}$, and $ig_{-fault-ad}$ respectively. To find out the above variables, i.e., ($I_{fault-ad}$, $\phi_{b-fault-ad}$, $\phi_{c-fault-ad}$, $\phi_{e-fault-ad}$, $\phi_{f-fault-ad}$, and $\phi_{g-fault-ad}$), and thus find out the new distribution of the stator current in the case of a type-III two-phase fault, the following steps are carried out.

Firstly, Equation (4) is substituted into Equation (23), yielding:

$$\frac{7}{2} * \bar{I}m * e^{i\Omega t} = e^{i\psi} * (ib_{-fault-ad} + ic_{-fault-ad} * e^{i\psi} + ie_{-fault-ad} * e^{3i\psi} + if_{-fault-ad} * e^{4i\psi} + ig_{-fault-ad} * e^{5i\psi} \quad (24)$$

Then, Equation (24) can be expressed using trigonometric formulas as follows:

$$\frac{7}{2} * \bar{I}m = I_{fault_ad} * \left((\cos\psi) * \cos\left(\phi_{b-fault-ad}\right) + (\cos 2\psi) * \cos\left(\phi_{c-fault-ad}\right) + (\cos 4\psi) * \cos\left(\phi_{e-fault-ad}\right) + (\cos 5\psi) * \cos\left(\phi_{f-fault-ad}\right) + (\cos 6\psi) * \cos\left(\phi_{g-fault-ad}\right)\right) \quad (25)$$

$$0 = I_{fault-ad} * ((\cos\psi) * \sin(\phi_{b-fault-ad}) + (\cos 2\psi) * \sin(\phi_{c-fault-ad}) + (\cos 4\psi) * \sin(\phi_{e-fault-ad}) + (\cos 5\psi) * \sin(\phi_{f-fault-ad}) + (\cos 6\psi) * \sin(\phi_{g-fault-ad})) \quad (26)$$

$$\frac{7}{2} * \bar{I}m = I_{fault-ad} * \left((\sin\psi) * \sin\left(\phi_{b-fault-ad}\right) + (\sin 2\psi) * \sin\left(\phi_{c-fault-ad}\right) + (\sin 4\psi) * \sin\left(\phi_{e-fault-ad}\right) + (\sin 5\psi) * \sin\left(\phi_{f-fault-ad}\right) + (\sin 6\psi) * \sin\left(\phi_{g-fault-ad}\right)\right) \quad (27)$$

$$0 = I_{fault-ad} * ((\sin\psi) * \cos(\phi_{b-fault-ad}) + (\sin 2\psi) * \cos(\phi_{c-fault-ad}) + (\sin 4\psi) * \cos(\phi_{e-fault-ad}) + (\sin 5\psi) * \cos(\phi_{f-fault-ad}) + (\sin 6\psi) * \cos(\phi_{g-fault-ad})) \quad (28)$$

Also, to keep the neutral current equal to zero after the faults, the following two Equations can be deduced:

$$0 = \cos(\phi_{b-fault-ad}) + \cos(\phi_{c-fault-ad}) + \cos(\phi_{e-fault-ad}) + \cos(\phi_{f-fault-ad}) + \cos(\phi_{g-fault-ad}) \quad (29)$$

$$0 = \sin(\phi_{b-fault-ad}) + \sin(\phi_{c-fault-ad}) + \sin(\phi_{e-fault-ad}) + \sin(\phi_{f-fault-ad}) + \sin(\phi_{g-fault-ad}) \quad (30)$$

Finally, solving Equations (25)–(30) using 'vpasolve ()' function in Matlab yields the new distribution of the remaining stator currents in the case of the failure in phases 'a' and 'd' as shown in Equation (31) and Figure 6a,b.

$$\begin{bmatrix} ia_{-fault\ ad} \\ ib_{-fault\ ad} \\ ic_{-fault\ ad} \\ id_{-fault\ ad} \\ ie_{-fault\ ad} \\ if_{-fault\ ad} \\ ig_{-fault\ ad} \end{bmatrix} = \begin{bmatrix} 0 \\ 1.562 * \bar{I}m * \cos(\omega t - 24.8°) \\ 1.562 * \bar{I}m * \cos(\omega t - 129.4°) \\ 0 \\ 1.562 * \bar{I}m * \cos(\omega t - 173.5°) \\ 1.562 * \bar{I}m * \cos(\omega t - 257.1°) \\ 1.562 * \bar{I}m * \cos(\omega t - 340.7°) \end{bmatrix} \quad (31)$$

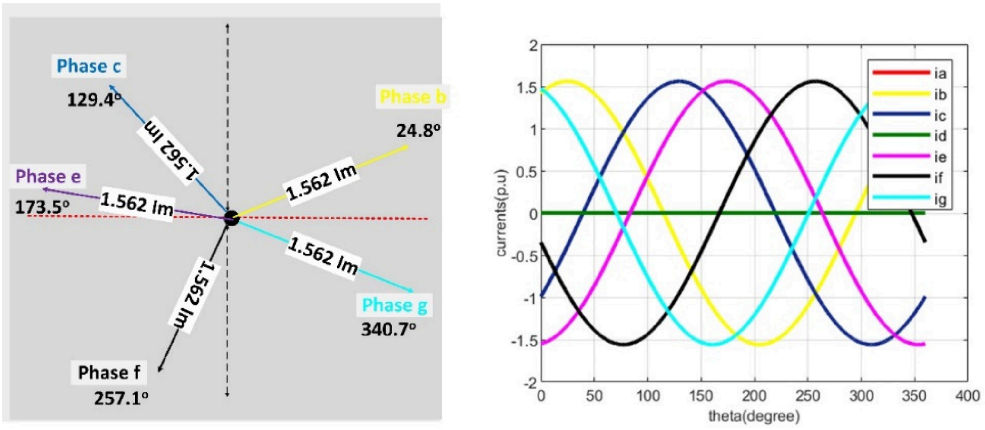

(**a**) (**b**)

Figure 6. Distribution of the currents in the seven-phase motor running under a type-III two-phase failure. (**a**) Phasor; (**b**) sinusoidal.

In summary, Figure 7 illustrates the fault-tolerant procedures that should be done to the stator currents under a type-III two-phase failure, i.e., ('a' and 'd'), in order to maintain the performance. Firstly, the amplitude of the remaining stator current should be increased by 56.2%. Then, phase 'b' that is opposite to the faulty phases is not shifted. After that, the two neighbor phases 'b' and 'c', should be shifted towards the faulty phases by 32.2° and 26.5° respectively. Finally, the two phases 'g' and 'e' that are opposite to the faulty phase should also be shifted towards the faulty phases by 26.5° and 32.2° respectively. This approach can be applied to all similar situations where faults occur in third-adjacent phases, such as phases 'a' and 'e', 'b' and 'f', and so on.

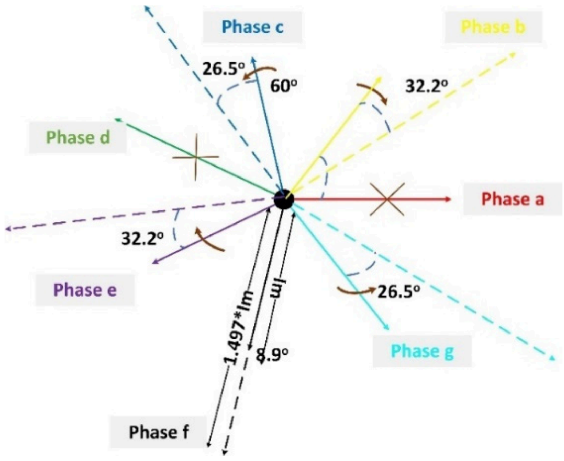

Figure 7. Phasor diagram illustrating the phase shift introduced to remaining healthy phase under a type-III two-phase failure.

It should be mentioned here that there will be an increase in the copper losses in the motor by a factor of 2.215 in the case of a type-I two-phase failure, 1.6 in the case of a type-II two-phase failure, and 1.7427 in the case of a type-III two-phase failure compared to the healthy operating conditions if the currents are controlled after, according to Equations (13), (22) and (31).

3. FTC Strategy for Seven-Phase Motor Drive Under Two-Phase Fault Conditions

3.1. SVPWM Control Strategy for a Seven-Phase Motor Drive Under Normal Operating Conditions

It is commonly understood that every third or fifth harmonic exists in the output of the seven-phase inverter, resulting in a significant amount of current in the stator coils of the seven-phase motor. This is due to the fact that these currents are only restricted by the stator impedance. To generate a clean sinusoidal output from the seven-phase inverter that is free from the third and fifth harmonics, multidimensional SVPWM is used, as shown in Figure 5 [31,32]. In this modulation technique, the six nearest voltage vectors of the reference voltage (V_ref) are utilized to generate V_ref in each sector, as shown in Figure 8a. These nearby vectors are calculated using the following equation:

$$Vs = \frac{2}{7}V_{DC}\left(sw_a + sw_b e^{i\psi} + sw_c e^{2i\psi} + sw_d e^{3i\psi} + sw_e e^{4i\psi} + sw_f e^{5i\psi} + sw_g e^{6i\psi}\right) \quad (32)$$

where sw_a, sw_b, sw_C, sw_D, sw_E, sw_F and sw_G are the PWM signals for the IGBTs in each leg of the seven-phase inverter. The PWM signals generated using this technique are shown in Figure 8b.

As mentioned earlier, when two phases are exposed to an open-circuit fault, the other phases should be phase-shifted to keep the motor running without losing performance. To adjust the current distribution after the fault, the output if the seven-phase inverter should also be reconfigured to match the new current setup. This means that the multidimensional SVPWM that is used for the seven-phase inverter in normal conditions cannot be applied after the faults, and hence the SVPWM should be modified after the faults to make the output of the seven-phase inverter match the new distribution of the currents. The novelty in this work is that it introduces a new SVPWM technique that takes into account the new distribution of the motor current after a fault in two phases and, at the same time, achieves the minimum inverter current. The new SVPWM techniques help the seven-phase inverter to generate output voltage signals that match the new current distribution for type-I, type-II,

and type-III two-phase failures. Additionally, this new technique also removes any third harmonic components from the inverter's output.

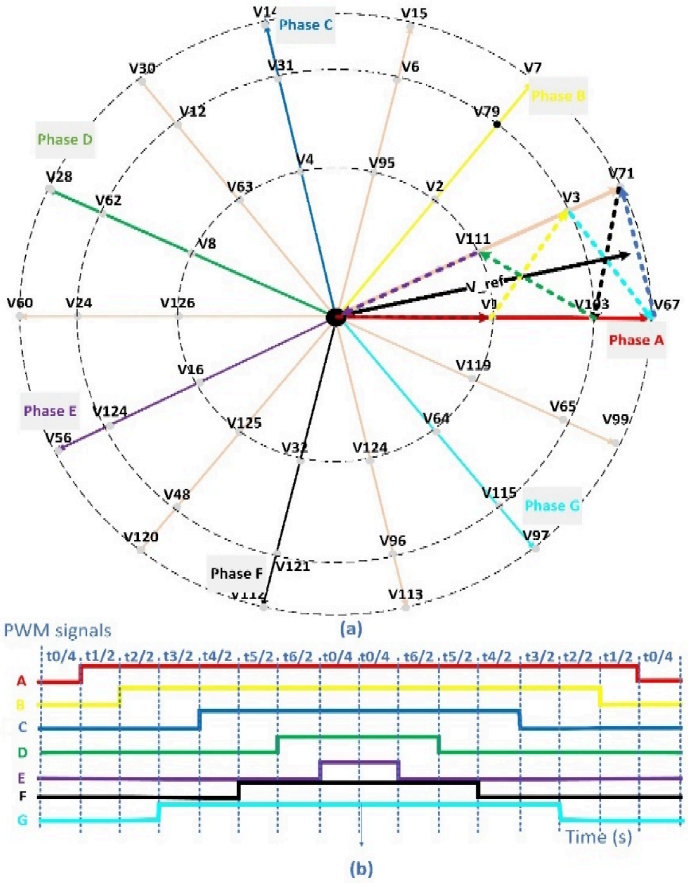

Figure 8. Seven-phase SVPWM in normal operation. (**a**) Space vector diagram, (**b**) PWM waveform.

3.2. SVPWM of the Seven-Phase Drive Under Two-Phase Failure

The first step is to map the fundamental component of V_ref into the orthogonal stationary frame α1-β1 as shown in Figures 9a, 10a, and 11a in the cases of a type-I two-phase failure, a type-II two-phase failure, and a type-III two-phase failure respectively. In addition to the map, the third component of V_ref into the orthogonal stationary frame α3-β3 is shown in Figures 9b, 10b, and 11b in the cases of a type-I two-phase failure, a type-II two-phase failure, and a type-III two-phase failure respectively. according to Equations (33)–(38).

$$Vs1_{fault-ab} = \frac{2}{7}V_{DC}\left(sw_c e^{i43.5^\circ} + sw_d e^{i142.6^\circ} + sw_e e^{i205.7^\circ} + sw_f e^{i268.8^\circ} + sw_g e^{i368.^\circ}\right) \quad (33)$$

$$Vs3_{fault-ab} = \frac{2}{7}V_{DC}\left(sw_c e^{i3*43.5^\circ} + sw_d e^{i3*142.6^\circ} + sw_e e^{i3*205.7^\circ} + sw_f e^{i3*268.8^\circ} + sw_g e^{i3*368.^\circ}\right) \quad (34)$$

$$Vs1_{fault-ac} = \frac{2}{7}V_{DC}\left(sw_b e^{i51.4^\circ} + sw_d e^{i122.6^\circ} + sw_e e^{i196.8^\circ} + sw_f e^{i266.1^\circ} + sw_g e^{i340.3^\circ}\right) \quad (35)$$

$$Vs3_{fault-ac} = \frac{2}{7}V_{DC}\left(sw_b e^{i3*51.4^\circ} + sw_d e^{i3*122.6^\circ} + sw_e e^{i3*196.8^\circ} + sw_f e^{i3*266.1^\circ} + sw_g e^{i3*340.3^\circ}\right) \quad (36)$$

$$Vs1_{fault-ad} = \frac{2}{7}V_{DC}\left(sw_b e^{i24.8^\circ} + sw_c e^{i129.5^\circ} + sw_e e^{i173.5^\circ} + sw_f e^{i257.1^\circ} + sw_g e^{i340.7^\circ}\right) \quad (37)$$

$$Vs3_{fault-ad} = \frac{2}{7}V_{DC}\left(sw_b e^{i3*24.8^\circ} + sw_c e^{i3*129.5^\circ} + sw_e e^{i3*173.5^\circ} + sw_f e^{i3*257.1^\circ} + sw_g e^{i3*340.7^\circ}\right) \quad (38)$$

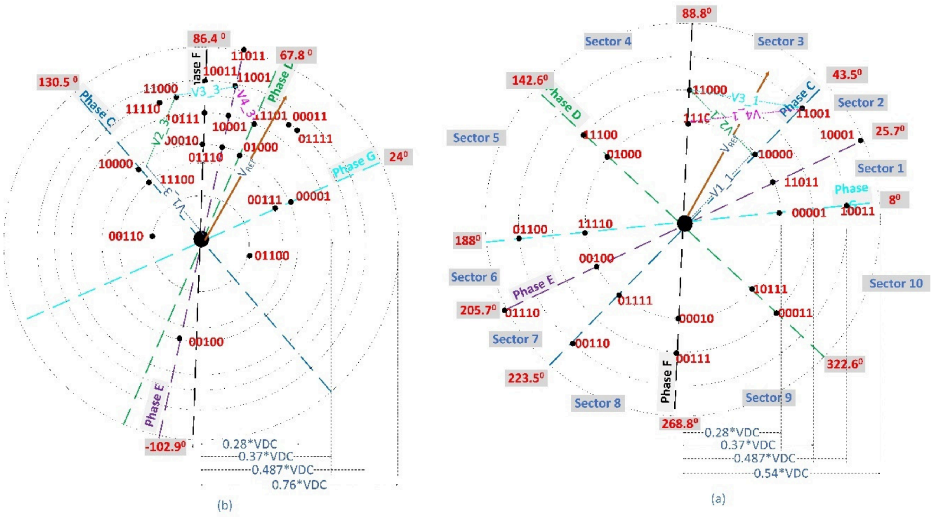

Figure 9. Voltage vector space distribution for a seven-phase motor drive under type-I two-phase failure ('a' and 'b') in (**a**) α1-β1 plan and (**b**) α3-β3 plan.

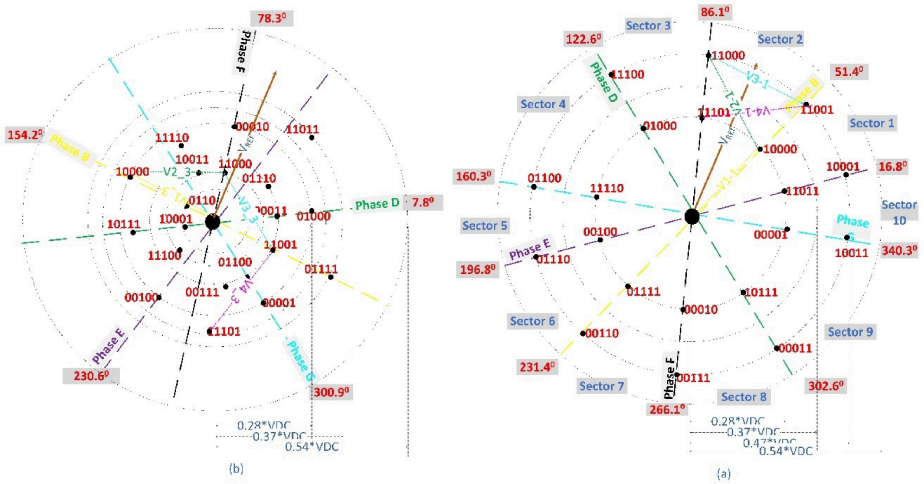

Figure 10. Voltage vector space distribution for a seven-phase motor drive under a type-II two-phase failure ('a' and 'c') in (**a**) α1-β1 plan and (**b**) α3-β3 plan.

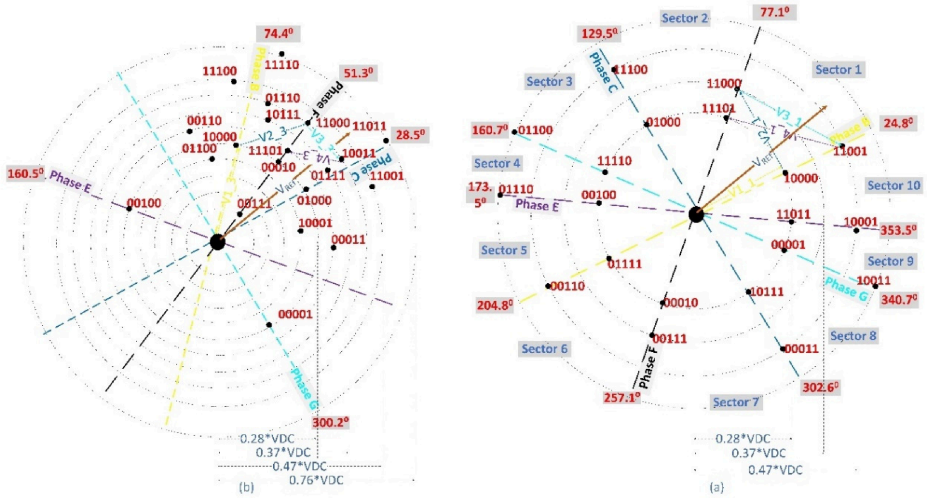

Figure 11. Voltage vector space distribution for a seven-phase motor drive under a type-III two-phase failure ('a' and 'd') in (**a**) α1-β1 plan and (**b**) α3-β3 plan.

It should be said here that there are other active vectors that can be obtained using Equations (33)–(38), but they are not shown in the figures because there are not of interest. It can be noticed also that vectors have different lengths. The lengths are 0.28*V_{DC}, 0.37*V_{DC}, 0.487*V_{DC}, 0.54*V_{DC}, and 0.76*V_{DC}.

The flowchart in Figure 12 shows the steps for using the new SVPWM method after two phases fail in a seven-phase drive. Here is what each part does: Firstly, the type of fault is identified based on the fault-flag signal. A 1 means everything is working normally, a 2 means there is a type-I two-phase failure between phases 'a' and 'b', a 3 means there is a type-II two-phase failure between 'a' and 'c', and a 4 means there is a type-III two-phase failure between 'a' and 'd'. It should be mentioned here that this signal is added to make the simulation more realistic. In real life this signal is obtained from the fault-detection and fault-phase-identification algorithms. This paper only concentrates on the fault-tolerant techniques after the detection and identification of the faulted phases. Then, the sector is chosen based on the position of V_ref and the fault-flag signal, as shown in Table 1.

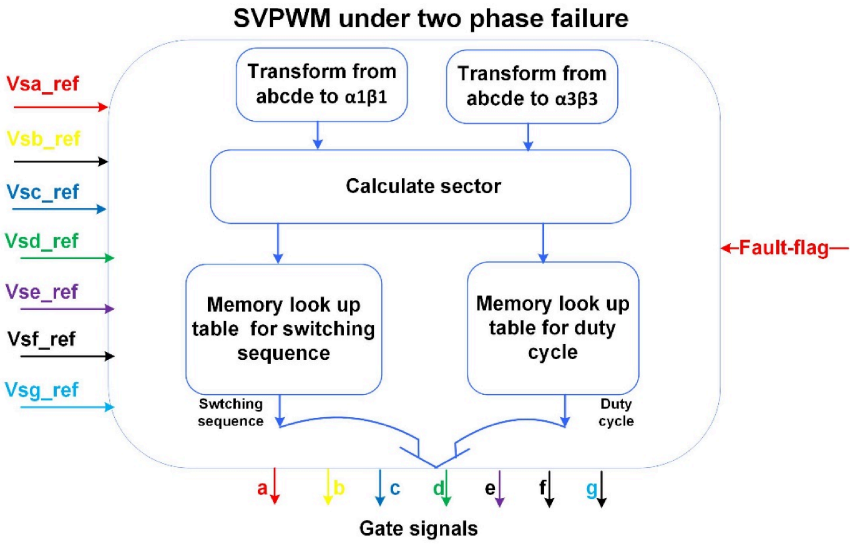

Figure 12. The flowchart illustrates the implementation of the new SVPWM after the loss of two phases.

Table 1. Selecting the sector.

Fault-Flag	V_ref Angle (θ)	Sector No	V_ref Angle (θ)	Sector No
2	$8° \leq \theta < 25.7°$	1	$188° \leq \theta < 205.7°$	6
	$25.7° \leq \theta < 43.5°$	2	$205.7° \leq \theta < 223.5°$	7
	$43.5° \leq \theta < 88.8°$	3	$223.5° \leq \theta < 268.6°$	8
	$88.8° \leq \theta < 142.6°$	4	$268.8° \leq \theta < 322.6°$	9
	$142.6° \leq \theta < 188°$	5	$322.6° \leq \theta < 8°$	10
3	$16.8° \leq \theta < 51.4°$	1	$196.8° \leq \theta < 231.4°$	6
	$51.4° \leq \theta < 86.1°$	2	$231.4° \leq \theta < 266.1°$	7
	$86.1° \leq \theta < 122.6°$	3	$266.1° \leq \theta < 302.6°$	8
	$122.6° \leq \theta < 160.3°$	4	$302.6° \leq \theta < 340.3°$	9
	$160.3° \leq \theta < 196.8°$	5	$340.3° \leq \theta < 16.8°$	10
4	$24.8° \leq \theta < 77.1°$	1	$204.8° \leq \theta < 257.1°$	6
	$77.1° \leq \theta < 129.5°$	2	$257.1° \leq \theta < 302.6°$	7
	$129.5° \leq \theta < 160.7°$	3	$302.6° \leq \theta < 340.7°$	8
	$160.7° \leq \theta < 173.5°$	4	$340.7° \leq \theta < 353.5°$	9
	$173.5° \leq \theta < 204.8°$	5	$353.5° \leq \theta < 24.8°$	10

Then, the time duration of each active vector is calculated. The paper is proposing a new approach to calculate the time duration of the active vectors besides the null vectors. This approach is straightforward and uses the four nearby active vectors near to V_ref in both α1-β1 and α3-β3 plans in each sector. It also helps to eliminate the third harmonic from the output of the seven-phase inverter. To illustrate the approach of this technique, Figure 13a–c are depicted. These figures illustrate how the four closest active vectors in the α1-β1 plan (V1_1, V2_1,V3_1,V4_1) and the four closest active vectors in the α3-β3 plan (V1_3, V2_3,V3_3,V4_3) are used to synthesize V_ref when it exists in the first sector in the case of a type-III two-phase failure ('a' and 'd'), while Figure 13b shows the SVPWM signal obtained using these vectors.

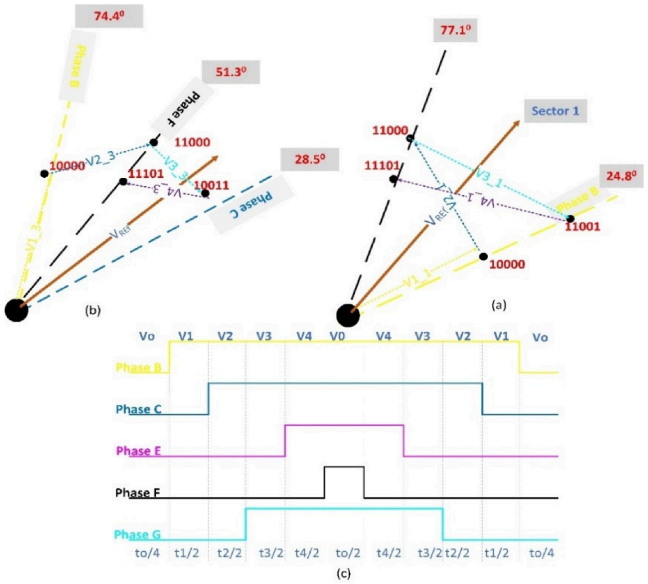

Figure 13. Illustration of how the four closely active vectors are used to synthesize V_ref in sector 1 using the new SVPWM technique in the case of a type-III two-phase failure ('a' and 'd'). (**a**) Active switching sequence in α1-β1 plan (**b**) and α3-β3 plan. (**c**) SVPWM signal.

The duration time, i.e., (t0, t1, t3, t3, and t4), of applying the four nearby active vectors can be calculated using the following equation based on Figure 13 [33]:

$$\begin{bmatrix} V\alpha 1_{ref} \\ V\beta 1_{ref} \\ V\alpha 3_{ref} \\ V\beta 3_{ref} \end{bmatrix} * \frac{T}{VDC} = \begin{bmatrix} V1_1\cos(24.8) & V2_1\cos(77.1) & V3_1\cos(24.8) & V4_1\cos(77.1) \\ V1_1\sin(24.8) & V2_1\sin(77.1) & V3_1\sin(24.8) & \mathrm{V4_1}\sin(77.1) \\ V1_3\cos(74.4) & V2_3\cos(51.3) & -V3_3\cos(3*24.8) & V4_1\cos(3*77.1) \\ V1_3\sin(74.4) & V2_3\sin(3*77.1) & -V3_3\sin(3*24.8) & V4_1\sin(3*77.1) \end{bmatrix} * \begin{bmatrix} t1 \\ t2 \\ t3 \\ t4 \end{bmatrix} \quad (39)$$

where $V\alpha 1_{ref}$, $V\beta 1_{ref}$, $V\alpha 3_{ref}$, and $V\beta 3_{ref}$ are the components of V_ref that are obtained by transforming V_ref into $\alpha_1\beta_1$, $\alpha_3\beta_3$ plans. T is the PWM period.

Solving the above equation yields:

$$\begin{bmatrix} t1 \\ t2 \\ t3 \\ t4 \end{bmatrix} = \mathrm{A} * \begin{bmatrix} V\alpha 1_{ref} \\ V\beta 1_{ref} \\ V\alpha 3_{ref} \\ V\beta 3_{ref} \end{bmatrix} \quad (40)$$

$$t0 = T - t1 - t2 - t3 - t4 \quad (41)$$

where

$$A = \frac{VDC}{T} * inverse(\begin{bmatrix}\begin{bmatrix} V1_1cos(24.8) & V2_1cos(77.1) & V3_1cos(24.8) & V4_1cos(77.1) \\ V1_1sin(24.8) & V2_1sin(77.1) & V3_1sin(24.8) & V4_1sin(77.1) \\ V1_3cos(74.4) & V2_3cos(51.3) & -V3_3cos(3*24.8) & V4_1cos(3*77.1) \\ V1_3sin(74.4) & V2_3sin(3*77.1) & -V3_3sin(3*24.8) & V4_1sin(3*77.1) \end{bmatrix}\end{bmatrix}) \quad (42)$$

$$A = \begin{bmatrix} +1.11 & -0.25 & -5.29 & 4.24 \\ -0.84 & +1.82 & +3.89 & -1.08 \\ +1.95 & -0.44 & +3.15 & -2.52 \\ -0.48 & +1.04 & -3.15 & 1.82 \end{bmatrix} \quad (43)$$

The dwell time and the switching sequence for each sector can be found in Table 2 when the new SVPWM is applied. It should be mentioned here that the drive cannot work at the rated load and the rated condition after the fault since the currents will be higher than the rated values and so $V\alpha 1_{ref}$,$V\beta 1_{ref}$. This means that the dwell time will be negative. Hence, there is a limit for $V\alpha 1_{ref}$, $V\beta 1_{ref}$ inside the algorithm of the SVPWM.

Table 2. Timing and switching order in each sector in the new SVPWMs.

Sector	Matrix A			Switching Order
	Fault_Signal = 2	**Fault_Signal = 3**	**Fault_Signal = 4**	
1	$\begin{bmatrix} 1.2 & -2.5 & 3.2 & -0.7 \\ -0.7 & 5.0 & 0.80 & 1.7 \\ 2.2 & -4.6 & -1.90 & 0.4 \\ -0.4 & 2.8 & 1.3 & -3.0 \end{bmatrix}$	$\begin{bmatrix} -0.4 & 1.4 & -2.0 & 1.7 \\ 2.1 & -1.7 & -0.7 & -1.4 \\ -0.79 & 2.64 & 1.29 & -1.0 \\ 1.2 & -1.00 & 1.2 & 2.54 \end{bmatrix}$	$\begin{bmatrix} 1.11 & -0.25 & -5.29 & 4.24 \\ -0.84 & 1.82 & 3.89 & -1.08 \\ 1.95 & -0.44 & 3.15 & -2.52 \\ -0.48 & 1.04 & -3.15 & 1.82 \end{bmatrix}$	10000, 10001, 11001, 11011
2	$\begin{bmatrix} -1.2 & 2.6 & -3.2 & 0.7 \\ 3.5 & -3.7 & 1.5 & 1.3 \\ -2.2 & 4.6 & 1.9 & -0.4 \\ 2.0 & -2.1 & 2.4 & 2.1 \end{bmatrix}$	$\begin{bmatrix} 1.5 & -0.1 & -2.6 & 0.5 \\ -2.1 & 1.7 & 0.7 & 1.4 \\ 2.7 & -0.2 & 1.6 & -0.3 \\ -1.2 & 1.00 & -1.2 & -2.4 \end{bmatrix}$	$\begin{bmatrix} -1.11 & 0.25 & 5.35 & -4.29 \\ 1.54 & 1.27 & 1.94 & -3.59 \\ -1.95 & 0.44 & -3.15 & 2.56 \\ 0.88 & 0.72 & -3.26 & 6.03 \end{bmatrix}$	10000, 11000, 11001, 11101
3	$\begin{bmatrix} 1.2 & -0.02 & -3.7 & 0.2 \\ -1.5 & 1.6 & 1.7 & 1.8 \\ 2.3 & -0.05 & 2.2 & -0.1 \\ -0.9 & 0.9 & 2.8 & -2.4 \end{bmatrix}$	$\begin{bmatrix} -1.5 & 0.1 & 2.7 & -0.6 \\ 2.2 & 1.4 & -0.2 & 1.6 \\ -2.6 & 0.2 & -1.6 & 0.3 \\ 1.2 & 0.8 & 0.4 & -2.8 \end{bmatrix}$	$\begin{bmatrix} 0.57 & 1.65 & 2.26 & 1.41 \\ -2.36 & -1.94 & -0.75 & 1.39 \\ 1.01 & 2.89 & -1.34 & -0.84 \\ -1.35 & -1.11 & 1.27 & -2.34 \end{bmatrix}$	01000, 11000, 11100, 11101
4	$\begin{bmatrix} -1.0 & 0.02 & 8.2 & -0.5 \\ 1.1 & 1.5 & -4.5 & 1.8 \\ -1.9 & 0.04 & -4.8 & 0.3 \\ 0.6 & 0.8 & 7.6 & -3.1 \end{bmatrix}$	$\begin{bmatrix} 0.50 & 1.3 & 2.5 & 1.5 \\ -2.1 & -1.3 & 0.22 & -1.7 \\ 0.8 & 2.4 & -1.4 & -0.9 \\ -1.2 & -0.8 & -0.4 & 2.9 \end{bmatrix}$	$\begin{bmatrix} -1.35 & -3.86 & -3.63 & -2.27 \\ 0.81 & 7.11 & 0.85 & 2.4 \\ -2.37 & -6.76 & 2.16 & 1.35 \\ 0.46 & 4.06 & -1.43 & -4.04 \end{bmatrix}$	01000, 01100, 11100, 11110
5	$\begin{bmatrix} -0.1 & 1.2 & -1.5 & 3.5 \\ -1.3 & -1.7 & 2.0 & -0.8 \\ -0.3 & 2.2 & 0.9 & -2.0 \\ -0.7 & -1.0 & -3.5 & 1.4 \end{bmatrix}$	$\begin{bmatrix} -0.5 & -1.4 & -2.4 & -1.4 \\ -0.7 & 2.5 & 1.3 & -1.0 \\ -0.89 & -2.48 & 1.40 & 0.90 \\ -0.4 & 1.4 & -2.2 & 1.8 \end{bmatrix}$	$\begin{bmatrix} -0.73 & 1.58 & -2.57 & 0.72 \\ -0.34 & -3.03 & -0.53 & -1.5 \\ -1.28 & 2.77 & 1.53 & -0.43 \\ -0.19 & -1.73 & 0.89 & 2.51 \end{bmatrix}$	00100, 01100, 01110, 11110
6	$\begin{bmatrix} 0.4 & -2.8 & 1.3 & -3.0 \\ -2.2 & 4.6 & 1.9 & -0.4 \\ 0.7 & -5.0 & -0.8 & 1.8 \\ -1.2 & 2.6 & -3.2 & 0.7 \end{bmatrix}$	$\begin{bmatrix} -1.2 & 1.00 & -1.2 & -2.4 \\ 0.8 & -2.6 & -1.2 & 1.0 \\ -2.1 & 1.7 & 0.7 & 1.4 \\ 0.4 & -1.5 & 2.1 & -1.7 \end{bmatrix}$	$\begin{bmatrix} 0.48 & -1.04 & 6.52 & -1.83 \\ -1.95 & 0.45 & 3.14 & -2.53 \\ 0.84 & -1.82 & -3.88 & 1.09 \\ -1.11 & 0.25 & -5.28 & 4.25 \end{bmatrix}$	00100, 00110, 01110, 01111
7	$\begin{bmatrix} -2.0 & 2.0 & -2.5 & -2.1 \\ 2.2 & -4.6 & -1.9 & -0.4 \\ -3.5 & 3.7 & 1.5 & 1.2 \\ 1.2 & -2.6 & 3.2 & -0.7 \end{bmatrix}$	$\begin{bmatrix} 1.2 & -1.00 & 1.2 & 2.4 \\ -2.7 & 0.2 & -1.6 & 0.3 \\ 2.1 & -1.7 & -0.7 & -1.4 \\ -1.6 & 0.1 & 2.6 & -0.6 \end{bmatrix}$	$\begin{bmatrix} -0.88 & -0.72 & -3.25 & 6.04 \\ 1.95 & -0.44 & -3.18 & 2.56 \\ -1.54 & -1.27 & 1.94 & -3.6 \\ 1.11 & -0.25 & 5.34 & -4.3 \end{bmatrix}$	00010, 00110, 00111, 01111
8	$\begin{bmatrix} 0.8 & -0.9 & 2.9 & 2.4 \\ -2.2 & 0.04 & -2.2 & -0.1 \\ 1.5 & -1.6 & -1.7 & -1.4 \\ -1.2 & 0.02 & 3.7 & 0.2 \end{bmatrix}$	$\begin{bmatrix} -1.2 & -0.8 & -0.4 & 2.8 \\ 2.6 & -0.2 & 1.6 & -0.3 \\ -2.2 & -1.4 & 0.2 & -1.6 \\ 1.4 & -0.10 & -2.7 & 0.6 \end{bmatrix}$	$\begin{bmatrix} 1.35 & 1.11 & 1.26 & -2.35 \\ -1.01 & -2.89 & -1.35 & -0.84 \\ 2.36 & 1.94 & -0.75 & 1.4 \\ -0.58 & -1.65 & 2.26 & 1.41 \end{bmatrix}$	00010, 00011, 10011, 10111

Table 2. *Cont.*

Sector	Matrix A			Switching Order
	Fault_Signal = 2	**Fault_Signal = 3**	**Fault_Signal = 4**	
9	$\begin{bmatrix} -0.7 & -0.9 & -7.6 & 3.1 \\ 1.9 & -0.04 & 4.8 & -0.3 \\ -1.1 & -1.5 & 4.5 & -1.9 \\ 1.0 & -0.02 & -8.2 & -0.5 \end{bmatrix}$	$\begin{bmatrix} 1.2 & 0.80 & 0.4 & -2.8 \\ -0.9 & -2.4 & 1.4 & 0.9 \\ 2.1 & 1.4 & -0.2 & 1.6 \\ -0.5 & -1.3 & -2.5 & -1.5 \end{bmatrix}$	$\begin{bmatrix} -0.46 & -4.06 & -1.44 & -4.04 \\ 2.37 & 6.76 & 2.17 & 1.35 \\ -0.81 & -7.11 & 0.86 & 2.4 \\ 1.35 & 3.86 & -3.64 & -2.26 \end{bmatrix}$	00001, 00011, 10011, 10111
10	$\begin{bmatrix} 0.7 & 1.0 & 3.5 & -1.4 \\ 0.30 & -2.1 & -0.9 & 2.0 \\ 1.3 & 1.7 & -2.0 & 0.8 \\ 0.2 & -1.2 & 1.6 & -3.5 \end{bmatrix}$	$\begin{bmatrix} 0.4 & -1.4 & 2.2 & -1.8 \\ 0.9 & 2.4 & -1.4 & -0.9 \\ 0.8 & -2.5 & -1.3 & 1.0 \\ 0.5 & 1.4 & 2.4 & 1.44 \end{bmatrix}$	$\begin{bmatrix} 0.19 & 1.73 & 0.9 & 2.51 \\ 1.28 & -2.76 & 1.53 & -0.42 \\ 0.34 & 3.02 & -0.53 & -1.5 \\ 0.73 & -1.58 & -2.57 & 0.72 \end{bmatrix}$	00001, 10001, 10011, 11011

It should be mentioned here that the FTC algorithm using the modified SVPWM in the case of the fault in phases 'a' and 'c' was introduced firstly in [33], but the paper has only dealt with the fault in phases 'a' and 'c'. This paper has introduced the algorithms for the FTC for type-I, type-II, and type-III two-phase failures.

4. Simulation Results for Seven-Phase Motor Drive After the Two-Phase Fault

4.1. Simulation for the Proposed SVPWM

The proposed SVPWM technique was simulated using SABER simulator to check if it is working properly based on the test demonstrated in Figure 14a for type-I two-phase failure, Figure 15a for type-II two-phase failure, and Figure 16a for type-III two-phase failure. It should be mentioned here that the reference voltages in these tests were shifted based on the new distribution of the healthy currents in each case. The results obtained from these tests are depicted in Figures 14b, 15b and 16b for type-I two-phase failure, type-II two-phase failure, and type-III two-phase failure respectively. The results demonstrate that the reference signals and the out filtered signals were almost identical. Also the figures show that the phase shift between the signals is almost equal to those obtained in Figures 2, 4 and 6 based on the proposed FTC technique.

For example, the phase shift between phase G and phase C in type-I two-phase failure can be calculated from Figure 14b as follows: $(1.2272 - 1.1976)/(1.5272 - 1.2272) * 360 = 35.5°$ which is equal to the phase shift between phase C (43.5°) and phase C (8°) in Figure 2. The phase shift in the other phases can be checked in the same way. It is found from the results in Figure 14b that the proposed SVPWM technique for type-I two-phase failure will generate voltage distribution and hence current distribution very similar to what proposed in Figure 2 and required in the proposed FTC technique.

Another example is that the phase shift between phase D and phase E in type-II two-phase failure can be calculated from Figure 15b as follows: $(1.0598 - 0.99305)/(1.2337 - 0.93375) * 360° = 74.2°$ which is very close to the phase shift between phase D (122.6°) and phase E (196.8°) in Figure 4. The phase shift in the other phases can be checked in the same way. The results in Figure 15b approve that the proposed SVPWM technique for type-II two-phase failure ('a' and 'c') will generate a voltage distribution and hence a current distribution very similar to that proposed in Figure 4 and required in the proposed FTC technique.

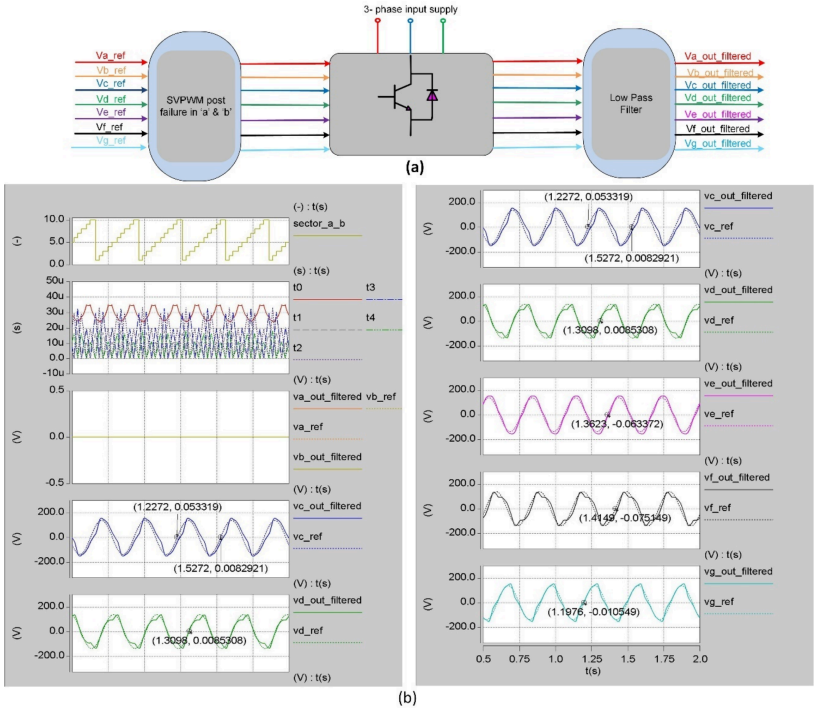

Figure 14. Simulation results obtained with proposed SVPWM for type-I two-phase failure ('a' and 'b'). (**a**) Test Setup Setup (**b**) The results.

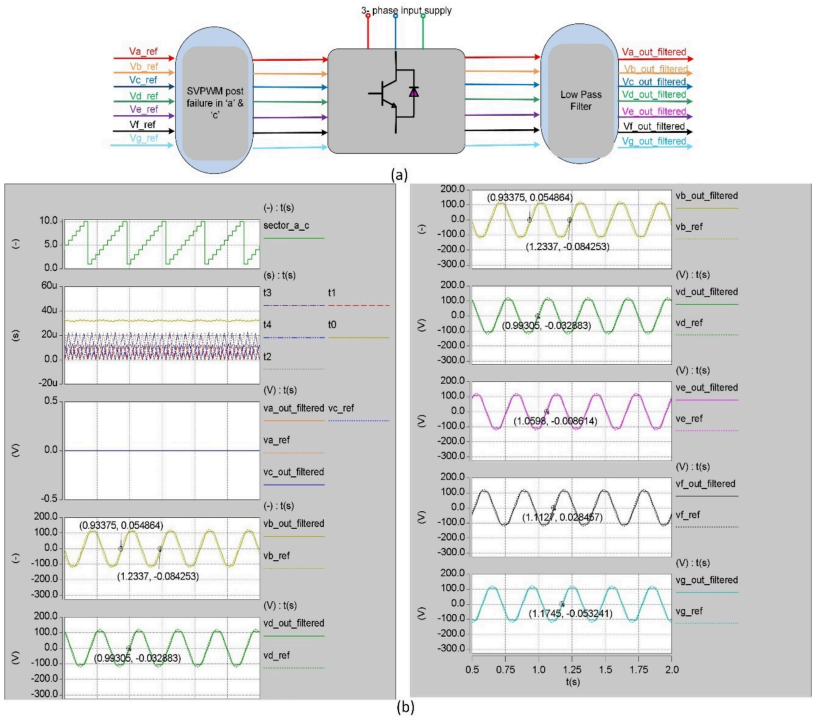

Figure 15. Simulation results obtained with proposed SVPWM for type-II two-phase failure ('a' and 'c'). (**a**) Test Setup Setup (**b**) The results.

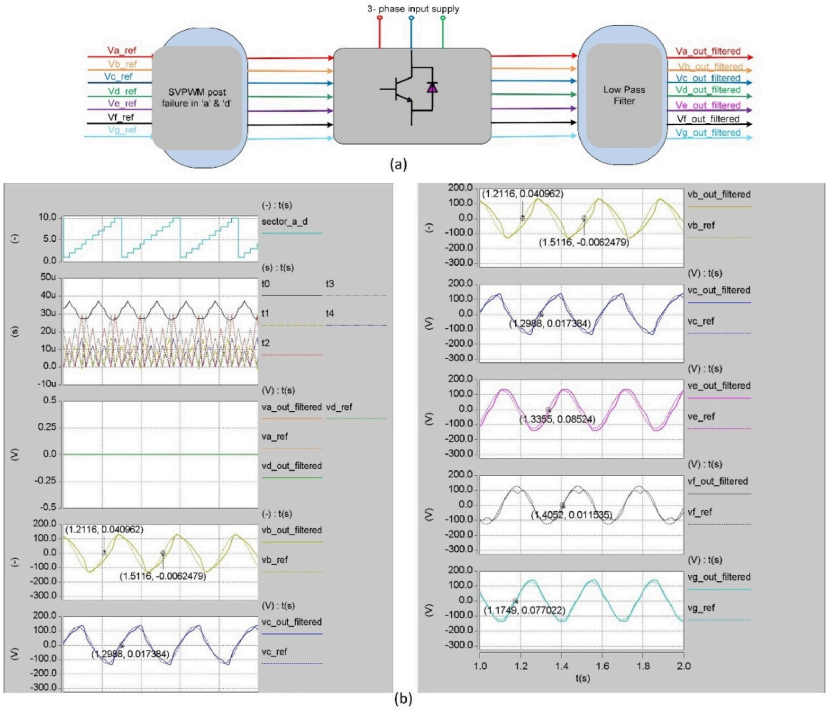

Figure 16. Simulation results obtained with proposed SVPWM for type-III two-phase failure ('a' and 'd'). (**a**) Test Setup (**b**) The results.

The final example is obtained from Figure 16b; the phase shift between phase E and phase F in type-III two-phase failure can be calculated as follows: $(1.4052 - 1.3355)/(0.3) * 360° = 83.64°$ which is very close to the phase shift between phase E (173.5°) and phase E (257.1°) in Figure 6. Finally, it can be concluded that the proposed SVPWM technique for type-III two-phase failure ('a' and 'd') will generate voltage distribution and hence current distribution very similar to what proposed in Figure 6 and required in the proposed FTC technique.

4.2. Simulation Results of the Enhancement in Torque and Speed Ripples Using the New SVPWM

To demonstrate the enhancement in both the torque and speed ripples achieved by implementing the new SVPWM techniques, the test depicted in Figure 17 was carried out using the SABER simulation platform. In this test the motor whose parameters is given in Appendix A was controlled using Field-Oriented Vector Control. The switching frequency was set to be 5KHz. The current controllers were designed with a 0.8 damping ratio and a bandwidth of 200 Hz. The speed controller was designed with a 0.8 damping ratio and a 10 Hz bandwidth. Moreover, the current controllers and the speed controllers will be the same before and after the fault. In this test, if the fault-flag signal is 1, the multidimensional SVPWM proposed in [31,32] will be implemented whether or not there is any fault. The SVPWM techniques that are proposed in this paper for type-I two-phase failure will be implemented in the case of a failure in phases 'a' and 'b' and when the fault-flag signal is 2. Moreover, the SVPWM techniques that are proposed in this paper for type-II two-phase failure will be implemented in the case of failure in phases 'a' and 'c' and the fault-flag signal is 3. Finally, the SVPWM techniques that are proposed in this paper for type-III two-phase failure will be implemented in the case of failure in phases 'a' and 'd' and the fault-flag signal is 4.

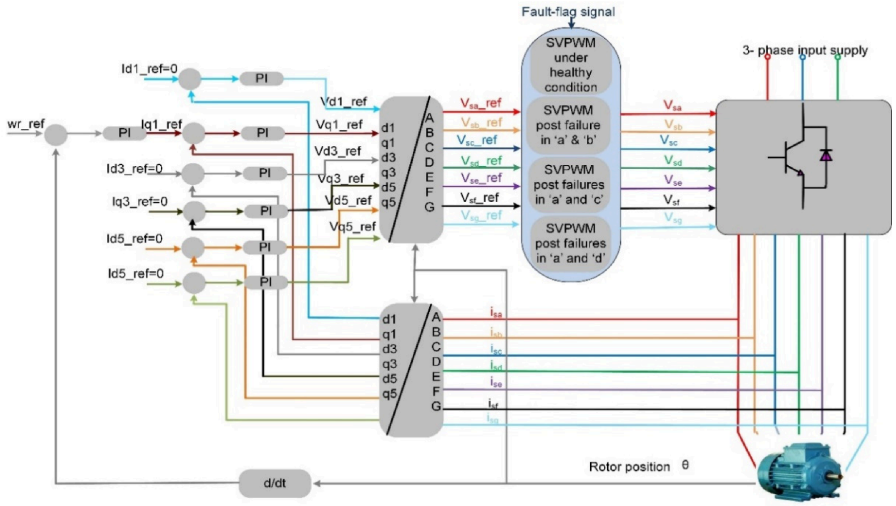

Figure 17. Field-Oriented Vector Control of the seven-phase drive after the failures in two phases.

The results from the test mentioned above are shown in Figures 18–21. In Figure 18 the motor was running without any fault and hence the SVPWM technique proposed in [31,32] was utilized till t = 2 s. from time t = 2 s till t = 3 s the motor was exposed to type-I two-phase failure (phase 'a' and 'b') and the fault-flag signal was still 1 which means that the SVPWM was not changed. After that, at t = 3 s, the fault-flag signal was changed to 2 which means that the new SVPWM proposed in this paper for this type of fault was utilized. The results show that the ripple in speed was 10 rpm before implementing the new SVPWM technique and reduced to 4 rpm after implementing the new SVPWM. Also the ripple in torque was reduced from 0.4 Nm to 0.1 Nm. Finally, implementing the new SVPWM helped to reduce the amplitude of currents 'ig' and 'ic' from 26 A to 23 A. The results confirm the improvements obtained by applying the new SVPWM in the case of a type-I two-phase failure (phase 'a' and 'b').

In Figure 19, the current Ic obtained from the test illustrated in Figure 18 was analyzed using MATLAB SIMULINK2020 powergui block to check the total harmonic distortion in the current under healthy conditions from t = 1 s till t = 2 s, after the fault in phases 'a' and 'b' without implementing the proposed FTC technique for type-I two-phase failure from t = 2 s till t = 3 s, and after implementing the proposed FTC technique for type-I two-phase failure from t = 3 s till t = 4 s. The THD was 0.13% under healthy conditions. It rises to 2.92% after the fault in phases 'a' and 'b' without implementing the proposed FTC technique for type-I two-phase failure. Finally, it rises to 3.03% after implementing the proposed FTC technique for type-I two-phase failure. The results show an increase in THD after implementing the proposed FTC technique for type-I two-phase failure. It should be mentioned here that the increase in THD after implementing the proposed FTC technique for type-I two-phase failure does not result from the increase in the harmonic. It results from a decrease in the current amplitude from 26.03 before implementing the proposed FTC technique to 23.52 after implementing the proposed FTC technique.

In Figure 20 the motor was running without any fault and the SVPWM technique proposed in [31,32] was utilized till t = 2 s. from time t = 2 s till t = 3 s the motor was subjected to type-II two-phase failure (phase 'a' and 'c') and the fault-flag signal was still 1 which means that the SVPWM was not changed. After that at t = 3 s, the fault-flag signal was changed to 3 which means that the new SVPWM proposed in this paper for this type of fault was utilized. The results show that the ripple in speed was 2 rpm before implementing the new SVPWM technique and reduced to 0.3 rpm after implementing the new SVPWM. Also the ripple in torque was reduced from 0.25 Nm to 0.1 Nm. Finally, implementing the

new SVPWM helped to reduce the amplitude of current 'ic' from 16.7 A to 12.3 A. The results confirm the improvements obtained by applying the new SVPWM in the case of a type-II two-phase failure (phase 'a' and 'c').

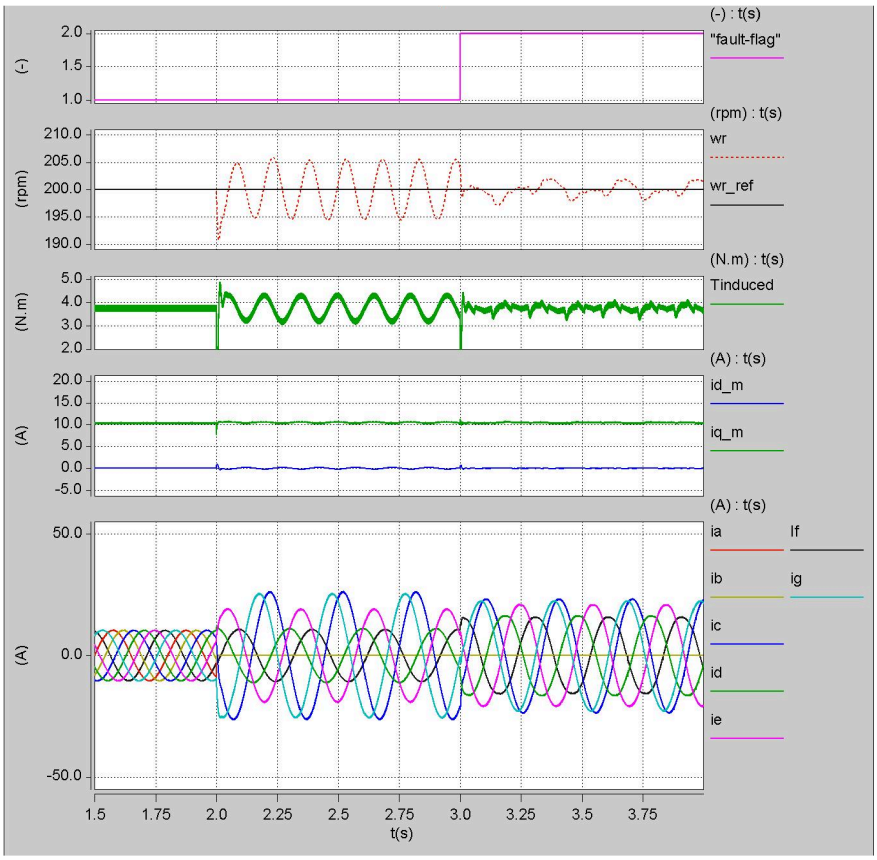

Figure 18. Simulation results of the enhancement in the speed and torque ripples when the proposed FTC developed for type-I two-phase failure ('a' and 'b') is applied.

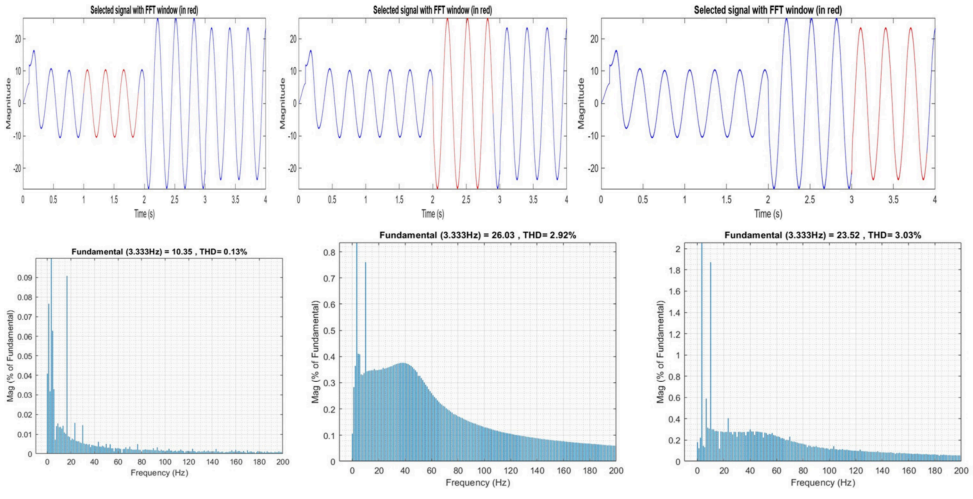

Figure 19. Simulation results of the THD before and after the implementation of the proposed FTC developed for type-I two-phase failure ('a' and 'b').

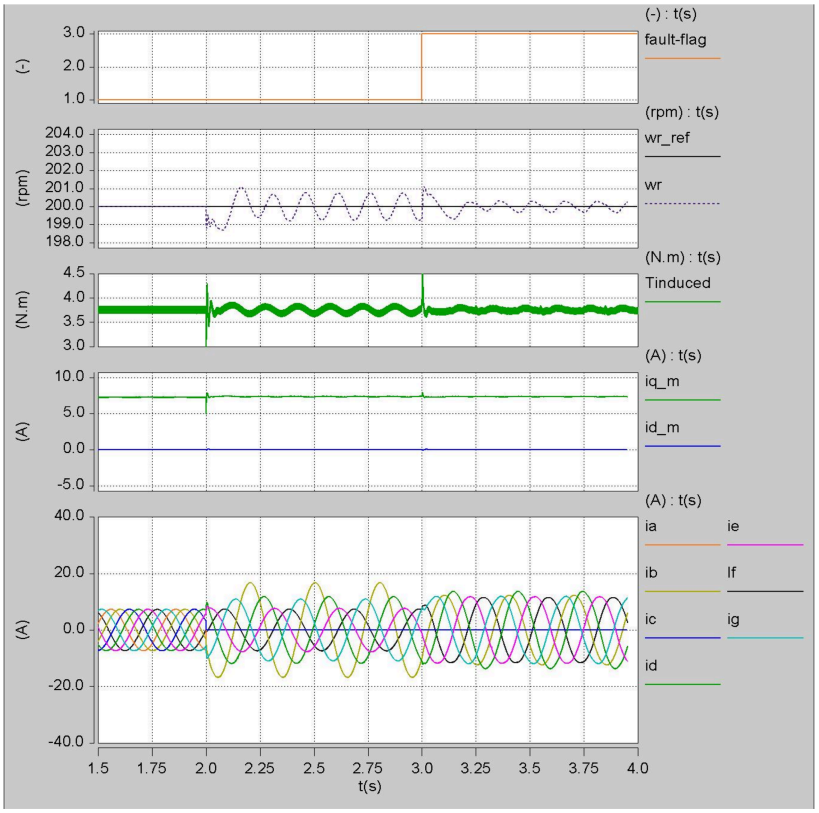

Figure 20. Simulation results of the enhancement in the speed and torque ripples when the proposed FTC developed for type-II two-phase failure (‘a’ and ‘c’) is applied.

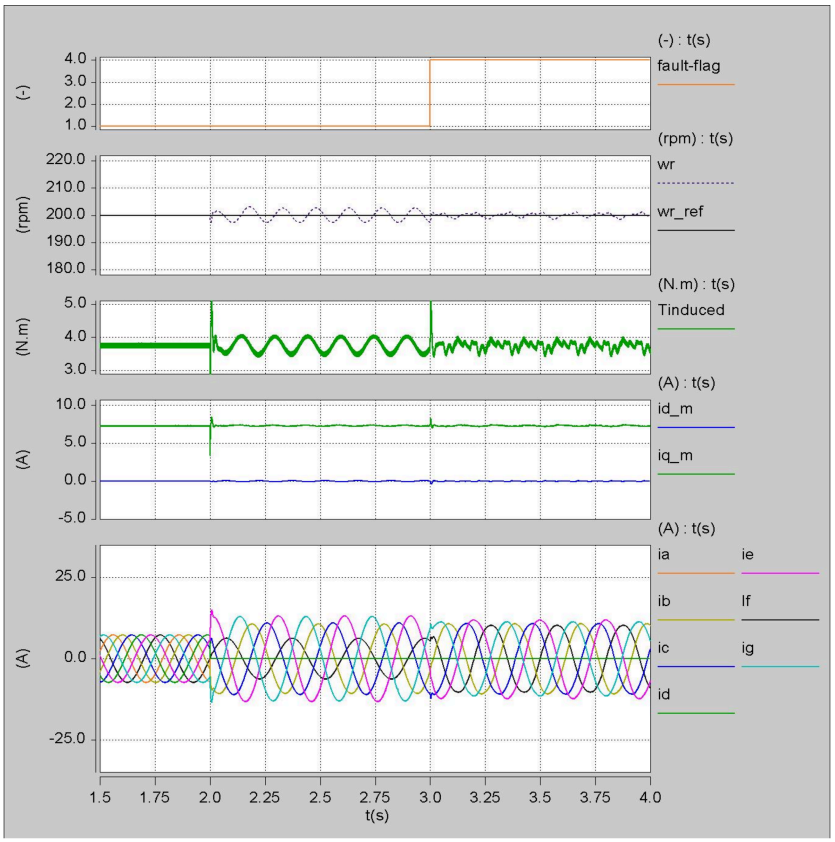

Figure 21. Simulation results of the enhancement in the speed and torque ripples when the proposed FTC developed for type-III two-phase failure (‘a’ and ‘d’) is applied.

In Figure 21 the motor was running without any fault and the SVPWM technique proposed in [31,32] was utilized till t = 2 s. from time t = 2 s till t = 3 s the motor was subjected to type-III two-phase failure (phase 'a' and 'd') and the fault-flag signal was still 1 which means that the SVPWM was not changed. After that at t = 3 s, the fault-flag signal was changed to 4 which means that the new SVPWM proposed in this paper for this type of fault was utilized. The results show that the ripple in speed was 5 rpm before implementing the new SVPWM technique and reduced to 0.5 rpm after implementing the new SVPWM. Also the ripple in torque was reduced from 0.6 Nm to 0.2. Finally, implementing the new SVPWM helped to reduce the amplitude of currents 'ig' and 'ie' from 13 A to 11 A Nm. The results confirm the improvements obtained by applying the new SVPWM in the case of a type-III two-phase failure (phase 'a' and 'd').

4.3. Simulation Results for the Speed and Loads Steps After the Fault in Two Phases

To demonstrate the stability and the dynamic response of the seven-phase drive system under two-phase faults after implementing the new SVPWM algorithms, the test illustrated in Figure 17 has been simulated on the SABER simulation platform, and the results of the tests are illustrated in Figures 22–24.

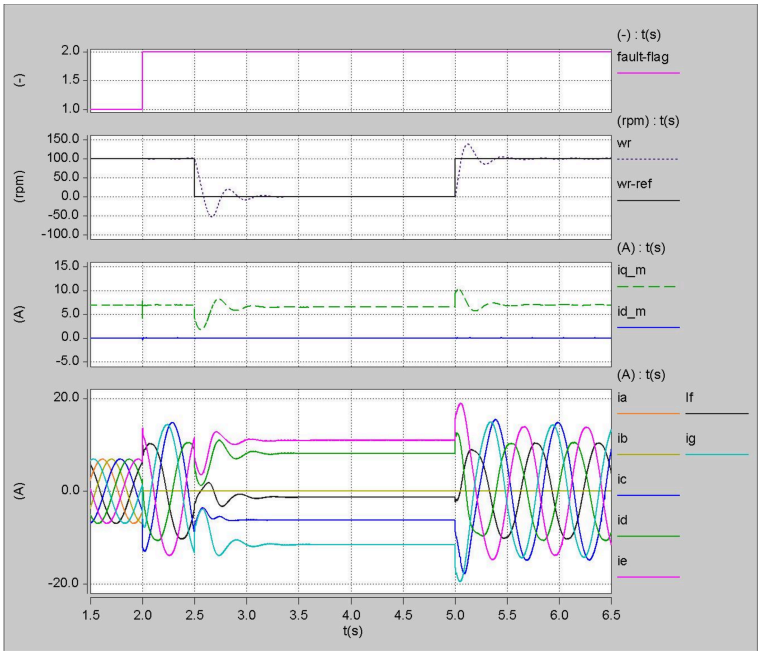

Figure 22. Simulation results of low-speed steps under type-I two-phase failure ('a' and 'b').

In Figure 22, the motor was running under healthy operating conditions, the fault-flag signal was 1, the speed was 100 rpm, and the load was 75% of the rated load condition. Then at t = 2 s, the motor was subjected to type-I two-phase failure (phase 'a' and 'b') and the fault-flag signal was changed to 2 simultaneously. After that at t = 2.5 s, the reference speed (wr-ref) was changed instantly to 0 rpm and stayed at 0 rpm till t = 5 s. Finally, at t = 5 s, wr-ref was changed to 100 rpm again. The results show that the motor responded to these steps in reference speeds with a good dynamic and steady-state responses and with a dynamic response very close to that obtained under healthy operating conditions.

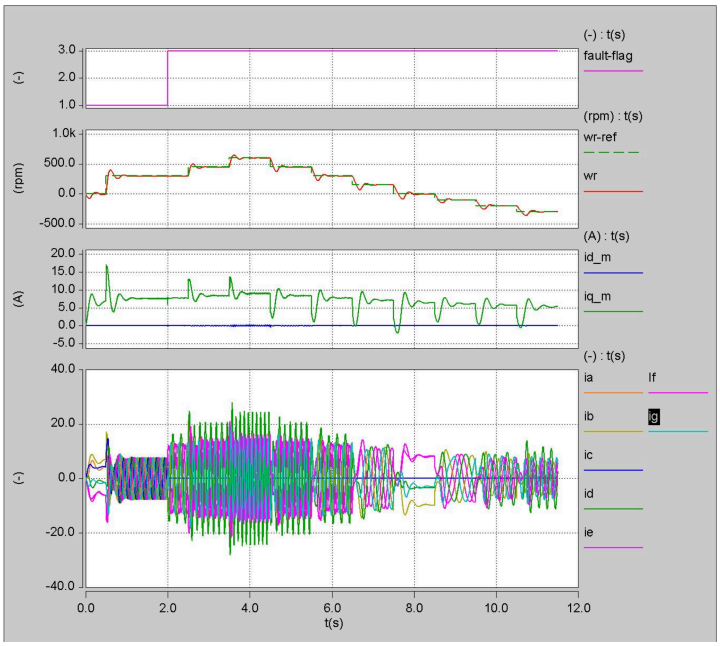

Figure 23. Simulation results of high-speed steps under a type-II two-phase failure (‘a’ and ‘c’).

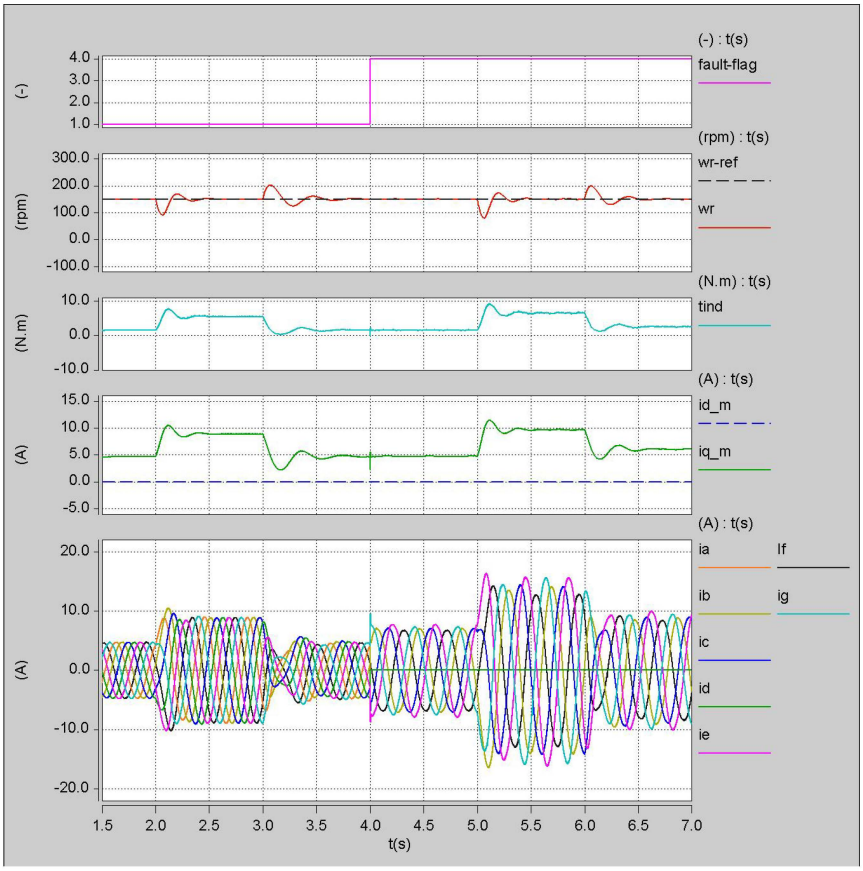

Figure 24. Simulation results of load steps under type-III two-phase failure (‘a’ and ‘d’).

In Figure 23, the motor was running under healthy operating conditions, the fault-flag signal was 1, the speed was zero, and the load was 75% of the rated load. At t = 0.5 s, wr-ref was changed to 300 rpm instantly. The motor responded to this speed step with good dynamic and steady-state response. Then at t = 2 s, the motor was exposed to type-II two-phase failure (phase ‘a’ and ‘c’) and the fault-flag signal was changed to 3 simultaneously.

After that, at t = 2.5 s, and t = 3.5 s, the reference speed (wr-ref) was changed instantly to 450 rpm and 600 rpm respectively. Then wr-ref was changed instantly to 450 rpm, 300 rpm, 150 rpm, 0 rpm, −100 rpm, −200 rpm, and −300 rpm at times t = 4.5 s, 5.5 s, 6.5 s, 7.5 s, 8.5 s, 9.5 s, 10.5 s respectively. The results illustrate that the motor responded to these steps in reference speeds with good dynamic and steady-state response. The results in Figure 23 prove that the motor drive is capable of responding to high-speed steps in the cases of a type-II two-phase failure (phase 'a' and 'c') very fast without compromising quality.

Finally, in Figure 24, the motor was running under healthy operating conditions, the fault-flag signal was 1, the speed was 150 rpm, and the load was 10% of the rated load. At t = 2 s, the load on the motor was increased instantly to be 80% of the rated load. The load on the motor is continued till t = 2 s. Then the load on the motor is returned instantly to be 10% of the rated load. Then at t = 4 s, the motor was subjected to type-III two-phase failure (phases 'a' and 'd') and the fault-flag signal was changed to 4 simultaneously. After that, at t = 5 s, the load on the motor was increased instantly again to be 80% of the rated load while the motor was running under a type-III two-phase failure (phases 'a' and 'd'). The load on the motor is continued till t = 6 s. Then the load on the motor is returned instantly to be 10% of the rated load. The results illustrate that the motor responded to these load disturbances while maintaining the speed. Also the results prove that the performance of the motor drive while the motor is exposed to type-III two-phase failure is almost similar to the response when the motor was running without faults.

5. Conclusions

This article has presented a novel fault-tolerant control (FTC) scheme for a seven-phase PMSM drive to enhance its performance when two phases experience an open-circuit failure at the same time. This approach makes the drive system more reliable and helps to reduce torque and speed fluctuations. To maintain the Magnetomotive Force (MMF) and improve overall performance, the FTC method focuses on controlling the current's magnitude and angle after the faults. The process starts by calculating the angles and magnitudes after the fault occurs in each scenario. Based on this new current distribution, a specific multidimensional SVPWM technique is designed for each fault case. When simulating the fault in phases "a" and "b", the torque ripple has decreased from 0.4 N·m to 0.1 N·m, and the speed ripple has dropped from 10 rpm to 4 rpm after applying the new FTC. For the fault in phases "a" and "c", the torque ripple has gone down from 0.25 N·m to 0.1 N·m, and the speed ripple has reduced from 2 rpm to 0.3 rpm with the new FTC. In the case of a fault in phases "a" and "d", the torque ripple has been cut from 0.6 N·m to 0.2 N·m, and the speed ripple has dropped from 5 rpm to 0.5 rpm after implementing the new FTC. Furthermore, the dynamic performance of the motor during faults and during changes in speed and load was just as good as when the motor was operating normally. The full comparison of the SVPWM-based technique proposed in this paper with the other fault techniques proposed in the literature including the reduced-order transformation-based SVPWM, optimized post-fault current reconfiguration, and Model Predictive Current Control (MPCC) is listed in Table 3 [8].

Table 3. Comparison between the new SVPWM-based technique and other fault-tolerant techniques.

Performance Index	Reduced-Order Transformation	SVPWM-Based	Optimized Post-Fault Current Reconfiguration	MPCC
Torque ripple %	Low–medium	Low	Very low	Very low
Speed ripple	Low–medium	Low	Very low	Very low

Table 3. *Cont.*

Performance Index	Reduced-Order Transformation	SVPWM-Based	Optimized Post-Fault Current Reconfiguration	MPCC
RMS phase current	Medium	Medium	Minimum/optimized	Low–medium
Maximum phase current	Medium	Medium	Explicitly constrained/minimized	Can be constrained
Copper loss	Medium	Medium	Minimum	Low–medium
THD	Medium	Low	Low–medium	Low with appropriate cost function
Switching frequency	Fixed if PWM used	Fixed	Fixed if followed by PWM	Usually variable in FCS-MPCC
DC-bus utilization	Depends on modulator	High	Depends on modulator	High, depending on vector set
Main strength	Simplification	Modulation quality	Current/loss optimization	Dynamic control

Funding: This research received no external funding.

Data Availability Statement: All data generated or analyzed during this study are included in this published article.

Conflicts of Interest: The author declare no conflict of interest.

Appendix A

The motor parameters are rated voltage = 400 V, rated speed = 1500 rpm, rated torque = 12 N·m, rated power = 2.15 kW, kt = 1.2 N·m/A, ke = 147 v/Krpm, Inertia = 20 kg/cm^2, R(ph-ph) = 4 Ω, and L(ph-ph) = 29.8 mH.

References

1. Villani, M.; Tursini, M.; Fabri, G.; Castellini, L. *Multi-Phase Fault Tolerant Drives for Aircraft Applications*; Electrical Systems for Aircraft, Railway and Ship Propulsion: Bologna, Italy, 2010; pp. 1–6. [CrossRef]
2. Wheeler, P.W. Multiphase induction motor drives. In Proceedings of the IET Chennai 3rd International on Sustainable Energy and Intelligent Systems (SEISCON 2012), Tiruchengode, India, 27–29 December 2012; p. 1. [CrossRef]
3. Subotic, I.; Bodo, N.; Levi, E.; Jones, M. Onboard Integrated Battery Charger for EVs Using an Asymmetrical Nine-Phase Machine. *IEEE Trans. Ind. Electron.* **2015**, *62*, 3285–3295. [CrossRef]
4. Yepes, A.G.; López Sánchez, Ó.; González-Prieto, I.; Durán, M.; Doval-Gandoy, J. A Comprehensive Survey on Fault Tolerance in Multiphase AC Drives, Part 1: General Overview Considering Multiple Fault Types. *Machines* **2022**, *10*, 208. [CrossRef]
5. Jia, H.; Yang, J.; Deng, R.; Wang, Y. Loss Investigation for Multiphase Induction Machine under Open-Circuit Fault Using Field–Circuit Coupling Finite Element Method. *Energies* **2021**, *14*, 5686. [CrossRef]
6. Munim, W.N.W.; Durán, M.; Che, H.; Bermúdez, M.; González-Prieto, I.; Rahim, N. A Unified Analysis of the Fault Tolerance Capability in Six-Phase Induction Motor Drives. *IEEE Trans. Power Electron.* **2017**, *32*, 7824–7836. [CrossRef]
7. Yang, G.; Hussain, H.; Li, S.; Yang, J. A Unified Fault-Tolerant Strategy for Multiphase Machine With Minimum Losses in Full Torque Operation Range Based on Closed-Form Expressions. *IEEE Trans. Power Electron.* **2022**, *37*, 12463–12473. [CrossRef]
8. Liu, X.; Liu, S.; Fu, Z.; Ge, L. A Critical Review of Fault-Tolerant Control for Multiphase PMSM Drive Systems. *IEEE Trans. Transp. Electrif.* **2025**, *11*, 13684–13704. [CrossRef]
9. Wang, X.; Wang, Z.; Xu, Z.; Cheng, M.; Wang, W.; Hu, Y. Comprehensive Diagnosis and Tolerance Strategies for Electrical Faults and Sensor Faults in Dual Three-Phase PMSM Drives. *IEEE Trans. Power Electron.* **2019**, *34*, 6669–6684. [CrossRef]
10. Pathania, A.; A, N.; Karampuri, R. Enhanced Fault-Tolerant Control for 9-Phase Induction Motor Drives in EVs. *Int. J. Multidiscip. Res.* **2025**, *7*, 1–13. [CrossRef]
11. Shi, P.; Wang, X.; Meng, X.; He, M.; Mao, Y.; Wang, Z. Adaptive Fault-Tolerant Control for Open-Circuit Faults in Dual Three-Phase PMSM Drives. *IEEE Trans. Power Electron.* **2023**, *38*, 3676–3688. [CrossRef]

12. González-Prieto, I.; Durán, M.; Barrero, F. Fault-Tolerant Control of Six-Phase Induction Motor Drives With Variable Current Injection. *IEEE Trans. Power Electron.* **2017**, *32*, 7894–7903. [CrossRef]
13. Sedrine, E.B.; Ojeda, J.; Gabsi, M.; Slama-Belkhodja, I. Fault-Tolerant Control Using the GA Optimization Considering the Reluctance Torque of a Five-Phase Flux Switching Machine. *IEEE Trans. Energy Convers.* **2015**, *30*, 927–938. [CrossRef]
14. Tian, B.; Hu, J.; Huang, X.; Zhou, B.; An, Q. Performance comparison of three types of PWM techniques for a Five-phase PMSM with a single-phase open circuited. In Proceedings of the 2021 13th International Symposium on Linear Drives for Industry Applications (LDIA), Wuhan, China, 1–3 July 2021; pp. 1–5. [CrossRef]
15. Chen, Q.; Liu, G.; Zhao, W.; Qu, L.; Xu, G. Asymmetrical SVPWM Fault-Tolerant Control of Five-Phase PM Brushless Motors. *IEEE Trans. Energy Convers.* **2017**, *32*, 12–22. [CrossRef]
16. Guzman, H.; Duran, M.J.; Barrero, F.; Zarri, L.; Bogado, B.; Prieto, I.G.; Arahal, M.R. Comparative Study of Predictive and Resonant Controllers in Fault-Tolerant Five-Phase Induction Motor Drives. *IEEE Trans. Ind. Electron.* **2016**, *63*, 606–617. [CrossRef]
17. Cheng, L.; Sui, Y.; Zheng, P.; Wang, P.; Wu, F. Implementation of Postfault Decoupling Vector Control and Mitigation of Current Ripple for Five-Phase Fault-Tolerant PM Machine Under Single-Phase Open-Circuit Fault. *IEEE Trans. Power Electron.* **2018**, *33*, 8623–8636. [CrossRef]
18. Zhou, H.; Zhao, W.; Liu, G.; Cheng, R.; Xie, Y. Remedial Field-Oriented Control of Five-Phase Fault-Tolerant Permanent-Magnet Motor by Using Reduced-Order Transformation Matrices. *IEEE Trans. Ind. Electron.* **2017**, *64*, 169–178. [CrossRef]
19. Chen, Q.; Zhao, W.; Liu, G.; Lin, Z. Extension of Virtual-Signal-Injection-Based MTPA Control for Five-Phase IPMSM Into Fault-Tolerant Operation. *IEEE Trans. Ind. Electron.* **2019**, *66*, 944–955. [CrossRef]
20. Chen, Q.; Gu, L.; Lin, Z.; Liu, G. Extension of Space-Vector-Signal-Injection-Based MTPA Control Into SVPWM Fault-Tolerant Operation for Five-Phase IPMSM. *IEEE Trans. Ind. Electron.* **2020**, *67*, 7321–7333. [CrossRef]
21. Bermudez, M.; Gonzalez-Prieto, I.; Barrero, F.; Guzman, H.; Kestelyn, X.; Duran, M.J. An Experimental Assessment of Open-Phase Fault-Tolerant Virtual-Vector-Based Direct Torque Control in Five-Phase Induction Motor Drives. *IEEE Trans. Power Electron.* **2018**, *33*, 2774–2784. [CrossRef]
22. Tian, B.; Mirzaeva, G.; An, Q.-T.; Sun, L.; Semenov, D. Fault-Tolerant Control of a Five-Phase Permanent Magnet Synchronous Motor for Industry Applications. *IEEE Trans. Ind. Appl.* **2018**, *54*, 3943–3952. [CrossRef]
23. Huang, W.; Hua, W.; Chen, F.; Yin, F.; Qi, J. Model Predictive Current Control of Open-Circuit Fault-Tolerant Five-Phase Flux-Switching Permanent Magnet Motor Drives. *IEEE J. Emerg. Sel. Top. Power Electron.* **2018**, *6*, 1840–1849. [CrossRef]
24. Zheng, L.; Fletcher, J.E.; Williams, B.W.; He, X. A Novel Direct Torque Control Scheme for a Sensorless Five-Phase Induction Motor Drive. *IEEE Trans. Ind. Electron.* **2011**, *58*, 503–513. [CrossRef]
25. Zhang, L.; Fan, Y.; Li, C.; Nied, A.; Cheng, M. Fault-Tolerant Sensorless Control of a Five-Phase FTFSCW-IPM Motor Based on a Wide-Speed Strong-Robustness Sliding Mode Observer. *IEEE Trans. Energy Convers.* **2018**, *33*, 87–95. [CrossRef]
26. Wang, X.; Jiang, H.; Shi, P.; Zhou, Y.; Xiao, D.; Wang, Z. Adaptive Fault-Tolerant Control-Based Fault Diagnosis of Dual Three-Phase PMSM Drives. *IEEE J. Emerg. Sel. Top. Power Electron.* **2025**, *13*, 2556–2564. [CrossRef]
27. Fu, J.R.; Lipo, T.A. Disturbance-free operation of a multiphase current-regulated motor drive with an opened phase. *IEEE Trans. Ind. Appl.* **1994**, *30*, 1267–1274. [CrossRef]
28. Parsa, L.; Toliyat, H. Sensorless Direct Torque Control of Five-Phase Interior Permanent-Magnet Motor Drives. *IEEE Trans. Ind. Appl.* **2007**, *43*, 952–959. [CrossRef]
29. Tani, A.; Mengoni, M.; Zarri, L.; Serra, G.; Casadei, D. Control of multi-phase induction motors with an odd number of phases under open circuit faults. *IEEE Trans. Power Electron.* **2012**, *27*, 565–577. [CrossRef]
30. Zhang, W.; Xu, D.; Enjeti, P.; Li, H.; Hawke, J.; Krishnamoorthy, H. Survey on Fault-Tolerant Techniques for Power Electronic Converters. *Power Electron. IEEE Trans.* **2014**, *29*, 6319–6331. [CrossRef]
31. Xue, S.; Wen, X.; Feng, Z. A Novel Multi-Dimensional SVPWM Strategy of Multiphase Motor Drives. In Proceedings of the 2006 12th International Power Electronics and Motion Control Conference, Portoroz, Slovenia, 30 August–1 September 2006; pp. 931–935. [CrossRef]
32. Wang, P.; Zheng, P.; Wu, F.; Zhang, J.; Li, T. Research on dual-plane vector control of fivephase fault-tolerant permanent magnet machine. In Proceedings of the 2014 IEEE Conference and Expo Transportation Electrification Asia-Pacific (ITEC Asia Pacific), Beijing, China, 31 August–3 September 2014; pp. 1–5. [CrossRef]
33. Saleh, K. Seven-Phase PMSM Drives Operation Post Two Types of Faults. *Appl. Sci.* **2022**, *12*, 7979. [CrossRef]

Disclaimer/Publisher's Note: The statements, opinions and data contained in all publications are solely those of the individual author(s) and contributor(s) and not of MDPI and/or the editor(s). MDPI and/or the editor(s) disclaim responsibility for any injury to people or property resulting from any ideas, methods, instructions or products referred to in the content.